Estudios Geológicos
enero-junio 2019, 75(1), e088
ISSN-L: 0367-0449
https://doi.org/10.3989/egeol.43438.515

The large eruption 4.2 ka cal BP in Cerro Blanco, Central Volcanic Zone, Andes: Insights to the Holocene eruptive deposits in the southern Puna and adjacent regions

La gran erupción de hace 4.2 ka cal en Cerro Blanco, Zona Volcánica Central, Andes: nuevos datos sobre los depósitos eruptivos holocenos en la Puna sur y regiones adyacentes

J.L. Fernandez-Turiel[1], F.J. Perez–Torrado[2], A. Rodriguez-Gonzalez[2], J. Saavedra[3], J.C. Carracedo[2], M. Rejas[1], A. Lobo[1], M. Osterrieth[4], J.I. Carrizo[5], G. Esteban[5], J. Gallardo[3], N. Ratto[6]

[1]Institute of Earth Sciences Jaume Almera, ICTJA, CSIC, Sole i Sabaris s/n, 08028 Barcelona, Spain. Email: jlfernandez@ictja.csic.es. ORCID ID: https://orcid.org/0000-0002-4383-799X, https://orcid.org/0000-0003-2356-0927, http://orcid.org/0000-0002-6689-2908

[2]Instituto de Estudios Ambientales y Recursos Naturales (i–UNAT), Universidad de Las Palmas de Gran Canaria (ULPGC), 35017 Las Palmas de Gran Canaria, Spain. ORCID ID: https://orcid.org/0000-0002-4644-0875, https://orcid.org/0000-0003-0688-0531, https://orcid.org/0000-0002-4282-2796

[3]IRNASA, CSIC, Cordel de Merinas 40–52, 37008 Salamanca, Spain. ORCID ID: https://orcid.org/0000-0003-0567-5499, https://orcid.org/0000-0002-4174-3930

[4]Instituto de Geología de Costas y del Cuaternario, Facultad de Ciencias Exactas y Naturales, Universidad Nacional de Mar del Plata–IIMYC–CONICET, Argentina. ORCID ID: https://orcid.org/0000-0001-9892-9923

[5]Facultad de Ciencias Naturales, Universidad Nacional de Tucumán, Miguel Lillo 205, 4000, San Miguel de Tucumán, Tucumán, Argentina. ORCID ID: https://orcid.org/0000-0003-1615-6408, https://orcid.org/0000-0001-6788-7513

[6]Instituto de las Culturas (IDECU), CONICET, Facultad de Filosofía y Letras, Universidad de Buenos Aires, Moreno 350, C1091 CABA, Argentina. ORCID ID: https://orcid.org/0000-0002-6862-3330

ABSTRACT

The eruption of the Cerro Blanco Volcanic Complex, in the southern Puna, NW Argentina dated at 4410–4150 a cal BP, was investigated to produce new information on stratigraphy, geomorphology, physical volcanology, radiocarbon dating, petrography, and geochemistry. Identification of pre–, syn–, and post–caldera products allowed us to estimate the distribution of the Plinian fallout during the paroxysmal syn–caldera phase of the eruption. The new results provide evidence for a major rhyolitic explosive eruption that spread volcanic deposits over an area of ~500,000 km^2, accumulating >100 km^3 of tephra (bulk volume). This last value exceeds the lower threshold of Volcanic Explosive Index (VEI) of 7. Ash-fall deposits mantled the region at distances >400 km from source and thick pyroclastic-flow deposits filled neighbouring valleys up to 35 km away. This eruption is the largest documented during the past five millennia in the Central Volcanic Zone of the Andes, and is probably one of the largest Holocene explosive eruptions in the world. We have also identified two additional rhyolitic eruptions in the region from two other eruptive sources: one during the Early–Holocene and another in the Late–Holocene. The identification and characterisation of these significant volcanic events provide new constraints into regional Holocene

Recibido el 4 de diciembre de 2018 / Aceptado el 25 de febrero de 2019 / Publicado online el 8 de mayo de 2019

Citation / Cómo citar este artículo: Fernandez-Turiel, J.L. et al. (2019). The large eruption 4.2 ka cal BP in Cerro Blanco, Central Volcanic Zone, Andes: Insights to the Holocene eruptive deposits in the southern Puna and adjacent regions. Estudios Geológicos 75(1): e088. https://doi.org/10.3989/egeol.43438.515

geological and archaeological records, and offer extensive regional chronostratigraphic markers over a wide geographical area of South America.

Keywords: Cerro Blanco Volcanic Complex; volcanic ash; Holocene; Central Volcanic Zone; Andes; Argentina.

RESUMEN

La erupción del Complejo Volcánico Cerro Blanco en el sur de la Puna, noroeste de Argentina (4410–4150 a BP) se investigó para obtener nueva información sobre estratigrafía, geomorfología, volcanología física, dataciones por radiocarbono, petrografía y geoquímica. La caracterización de los productos en relación a la evolución de la caldera de Cerro Blanco permitió estimar la distribución de los depósitos de ceniza de la fase paroxísmica Plineana de la erupción. Estos novedosos resultados evidencian una gran erupción explosiva riolítica que generó depósitos cineríticos en un área de aproximadamente 500.000 km^2, acumulando >100 km^3 de tefra (volumen total). Este último valor supera el umbral inferior del Índice de Explosividad Volcánica (IEV) de 7. Los depósitos de caída de ceniza cubrieron la región, llegando a más de 400 km desde el Complejo Volcánico de Cerro Blanco, y los potentes depósitos de flujos piroclásticos rellenaron los valles vecinos alcanzando una distancia de 35 km. Esta erupción es la más grande documentada durante los últimos cinco milenios en la Zona Volcánica Central de los Andes y es probablemente una de las mayores erupciones explosivas holocenas del mundo. Además, se han identificado otras dos erupciones riolíticas en la región procedentes de otros dos centros eruptivos: una durante el Holoceno temprano y otra en el Holoceno tardío. La identificación y caracterización de estos grandes eventos volcánicos proporcionan nuevas guías para los registros geológicos y arqueológicos regionales del Holoceno, siendo marcadores cronostratigráficos de aplicación a una extensa área geográfica de América del Sur.

Palabras clave: Complejo Volcánico Cerro Blanco; ceniza volcánica; Holoceno; Zona Volcánica Central; Andes; Argentina.

Introduction

Tephra is fragmental material produced by an explosive volcanic eruption. Larger tephra ('blocks' or 'bombs') follow ballistic trajectories and pose a local threat (usually < 5 km). However, lapilli (2 to 64 mm in diameter) and ash (< 2 mm in diameter) are convected upwards within the eruption column and dispersed by wind or buoyancy forces. Ash particles can be carried hundreds or even thousands of kilometres away from source, being the most frequent, and often widespread, volcanic hazard (Jenkins, S. F. *et al.*, 2015). In this way, tephra deposits form an isochron that directly links various sedimentary successions and enable us to synchronize and date geological, palaeoenvironmental or archaeological records (Lane *et al.*, 2017; Lowe, 2011; Ponomareva *et al.*, 2015). This is the rationale of the development of tephra studies and the establishment of tephrostratigraphy and tephrochronology. In addition, preserved tephra deposits are frequently used in the reconstruction of past volcanic eruptions and the evaluation of volcanic hazards to prevent the impact of similar eruptions possibly occurring in the future (Houghton, B. & Carey, R. J, 2015; Lowe, 2011).

In South America, the explosive Holocene volcanism is mainly produced by the Andean Volcanic Arc, along the Andean Cordillera, and is segmented into four main volcanic zones separated from each other by volcanic gaps (Stern, 2004): the Northern (NVZ), the Central (CVZ), the Southern (SVZ), and the Austral Volcanic Zone (AVZ) (Fig. 1). In this setting, although mostly concentrated in SVZ and AVZ, tephrochronology studies are of critical importance because would help in reconstructing dispersal of ash during past explosive eruptions providing potential stratigraphic markers that contribute toward establishing a chronological framework for a range of applications (e.g., palaeoenvironment, palaeoclimate, archaeology, and rates of geomorphic change) (Fontijn *et al.*, 2014; Stern, 2008).

Several previous studies have focused on the widespread ash-fall deposits found in the uppermost Quaternary sequences of NW Argentina (Hermanns & Schellenberger, 2008; Malamud *et al.*, 1996; Montero-López *et al.*, 2009; Ruggieri *et al.*, 2010; Trauth *et al.*, 2003).). These studies attributed these ash-fall deposits to eruptions from volcanoes located in the Central Volcanic Zone of the Andes but no reliable correlation to a specific source has been proposed (Hermanns & Schellenberger, 2008; Malamud *et al.*, 1996). This is mostly due to the lack of adequate geochemical data (e.g., single shards glass major and trace element composition, mineral chemistry) and reliable dating (often in contrast with each other) on proximal deposits of the potential

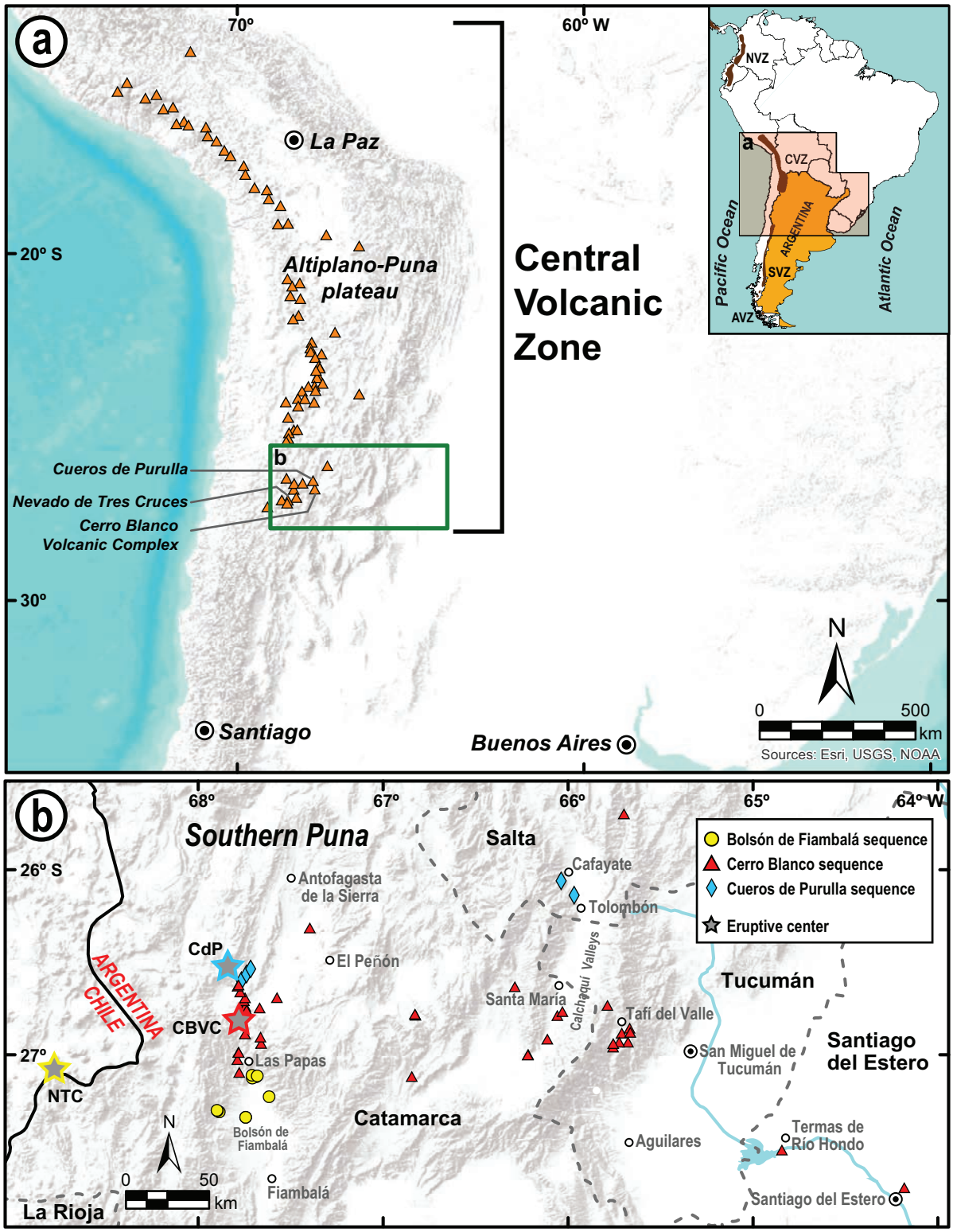

Figure 1.—(a) Holocene volcanic centres in the Andean Central Volcanic Zone (data from Global Volcanism Program, 2013a); NVZ, Northern Volcanic Zone; CVZ, Central Volcanic Zone; SVZ, Southern Volcanic Zone; and AVZ, Austral Volcanic Zone. (b) Studied sections and eruptive centres (CdP, Cueros de Purulla; CBVC, Cerro Blanco Volcanic Complex; NTC, Nevado Tres Cruces).

source volcanoes. This situation changed with the discovery of several upper Pleistocene deposits attributed to the Cerro Blanco Volcanic Complex (CBVC) (Arnosio *et al.*, 2008) and, particularly, with identification of Holocene deposits associated with the CBVC (Montero-López *et al.*, 2010a). In particular, the presence of Holocene volcanic deposits in the southern Puna led us to review all available data and to conduct new studies of recent pyroclastic fall deposits and ignimbrites in a large region in NW Argentina in order to better identify their sources (Fernandez-Turiel *et al.*, 2013, 2014, 2015). We present here the results of geomorphology, stratigraphy and geographical distribution of tephra deposits, the detailed characterization of tephra (including particle size, mineralogy, and geochemical composition), and the radiocarbon dating of these deposits to test their possible association with large Holocene eruptions in the CBVC. This work mainly focuses on details of the Cerro Blanco pyroclastic fall deposits and ignimbrites, but the stratigraphic study of regional distribution requires us to include the analysis of bracketing Cueros de Purulla (older) and Bolsón de Fiambalá (younger) ash deposits.

Geological setting

The 3500–4700 m high Cerro Blanco Volcanic Complex (CBVC) is part of the Cordillera de San Buenaventura in NW Argentina (26º 47' 24.46" S, 67º 45' 40.68" W) (Global Volcanism Program, 2013b). It overlies the Miocene to Pliocene La Hoyada Volcanic Complex (~7 to ~2 Ma), which consists of ignimbrites, lava domes, and lava flows (Montero-López *et al.*, 2010b). It is situated on the southern border of the Altiplano–Puna Plateau, in the Central Volcanic Zone of the Andes (Fig. 1a and b), where voluminous mafic and silicic Miocene–Quaternary calc–alkaline volcanism occurs within the plateau and along its margins (Bianchi *et al.*, 2013; Kay *et al.*, 2006, 2010). The underlying continental crust is composed of Palaeozoic–Mesozoic igneous and metasedimentary rocks (Montero-López *et al.*, 2010a).

Four calderas have been recognized in the CBVC (Fig. 2) ; from the oldest to the youngest: the less preserved El Niño Caldera (Arnosio *et al.*, 2005); the Pie de San Buenaventura Caldera (Montero-López *et al.*, 2009); the Robledo Caldera; and the Holocene Cerro Blanco Caldera (Báez *et al.*, 2015; Montero-López *et al.*, 2010a). The ages of the first three are unknown, and it was hypothesized that these calderas are part of one larger structure (Báez *et al.*, 2015). Activity from calderas of the Cerro Blanco Complex produced lava domes, pyroclastic density current (PDC) deposits, and pyroclastic fall deposits (Arnosio *et al.*, 2005; Báez, 2014; Báez *et al.*, 2015; Montero-López *et al.*, 2010b, 2010a; Roberge *et al.*, 2012; Seggiaro *et al.*, 2000). Radiocarbon ages obtained in peat levels underlying ignimbrites south of the youngest Cerro Blanco Caldera suggest they are younger than 5 ka BP (Montero-López *et al.*, 2009, 2010a).

In addition to the Cerro Blanco complex, there are several morphologically young–looking volcanoes in the region. The volcanic area of Nevado Tres Cruces, El Solo and Ojos del Salado (the world's highest volcano at 6893 m a.s.l.) (27°05'S, 68°45'W; Fig. 1b) includes extensive Pleistocene–Holocene high–silica pyroclastic-flow deposits from associated stratovolcanoes, volcanic domes, cones, and explosion craters (Baker *et al.*, 1987). The Cueros de Purulla volcano (CdP) (26°33'S, 67°49'W; Fig. 1b) is a rhyolitic lava dome with associated ignimbrites (Báez *et al.*, 2015; Kay *et al.*, 2008), located 25 km north of Cerro Blanco Caldera.

Methods

Identification, logging, and sampling of 62 outcrops of tephra sections and lava domes were performed during several field campaigns in a wide region of northwest Argentina (Fig. 1b), providing a set of more than 230 samples. The lithofacies descriptions are based on published methodologies (Branney & Kokelaar, 2002; Cas *et al.*, 2008).

Petrography was studied by optical and scanning electron microscopy on polished thin sections and grain mounts on carbon stubs. Groundmass glass, phenocrysts, microphenocrysts, and microlites of glass shards were analysed on polished thin sections by electron probe microanalyser (EPMA) (Fernandez-Turiel *et al.*, 2018a). Particle size distributions were determined in ash samples by laser diffraction (Fernandez-Turiel *et al.*, 2018b).

Radiocarbon dating was done by Accelerator Mass Spectrometry (AMS) in Beta Analytic Inc. and NSF-Arizona AMS Facility, University of Arizona. All samples were taken below the surface, visually checked under a microscope, and handpicked cleaned. The ^{14}C ages were calibrated to calendar years BP using Bayesian statistics with OxCal v4.3.2 [104] (round to the nearest 10) (Bronk Ramsey, 2009) with the

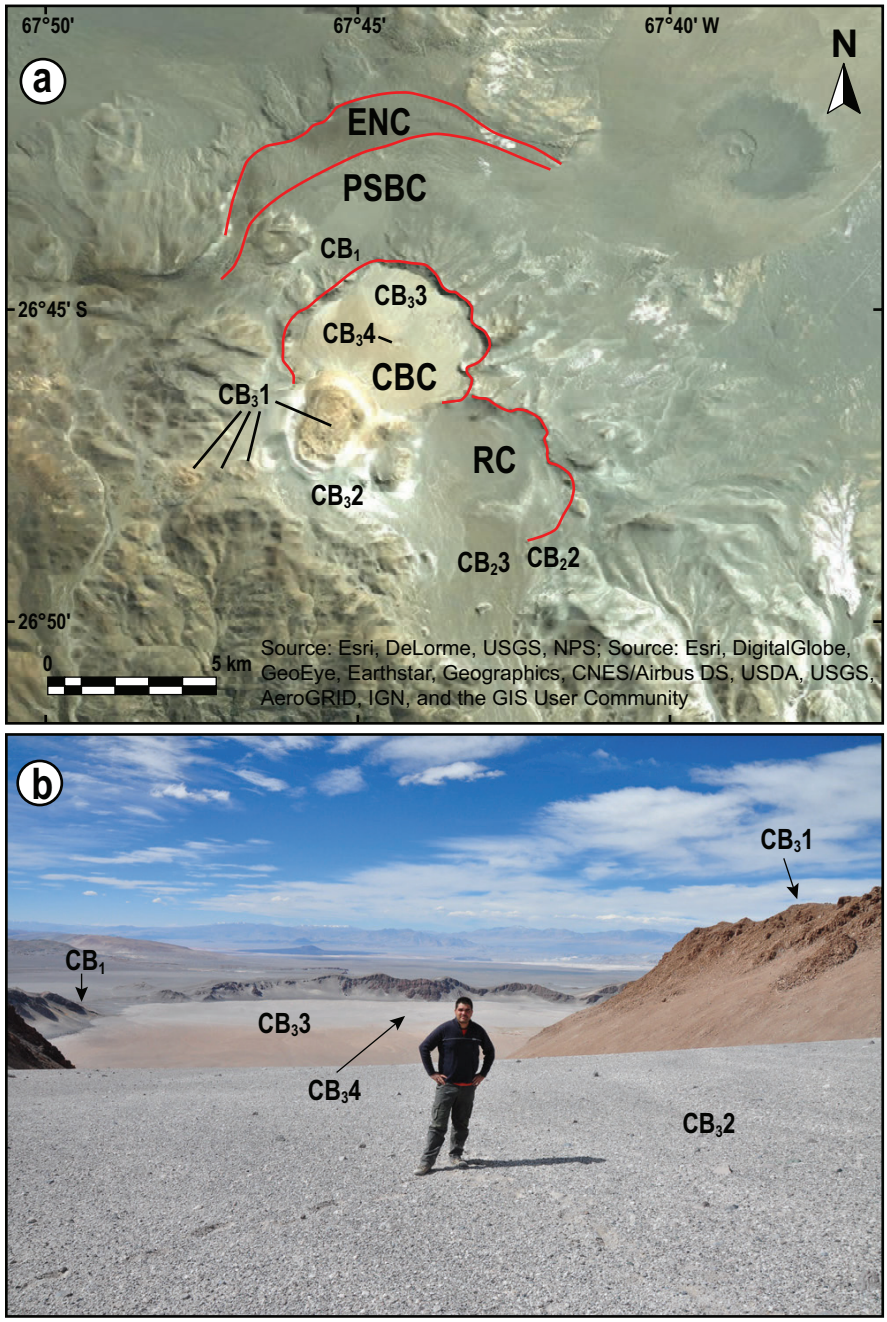

Figure 2.—(a) The Cerro Blanco Volcanic Complex showing the El Niño Caldera (ENC), the Pie de San Buenaventura Caldera (PSBC), the Robledo Caldera (RC), and the Cerro Blanco Caldera (CBC); (b) Cerro Blanco Caldera (down A. Rodriguez-Gonzalez). CB_1, pre–caldera block–and–ash flow deposits; $CB_2$2, Plinian ash-fall deposits; $CB_2$3, ignimbrites, $CB_3$1, lava–domes; $CB_3$2, lapilli fall deposits; $CB_3$3, post–caldera block–and–ash flow deposits; $CB_3$4, sinter deposits.

SHCal13 atmospheric curve (Hogg *et al.*, 2013) (Fernandez-Turiel *et al*., 2019; Table S1).

The widely-used, advection-diffusion type, tephra fall simulation model, Tephra2 (Bonadonna *et al.*, 2005; Connor & Connor, 2006), was used to model the paroxysmal phase of 4.2 ka cal BP eruption of CBVC. This deterministic modelling code allowed simulating affected area caused by CB_2 ash-fall. Tephra2 required three input datasets: a wind dataset, a grid dataset and a configuration dataset. The inverse problem method was used to

set the input variables. Wind data (1980-2012; n=12,054 days) were downloaded from NCEP/NCAR Reanalysis site for the coordinates of CBVC (26° 47' 24.46" S, 67° 45' 40.68" W). Different wind profiles were tested to be compatible with observations in the field (geographical distribution and ash layer thickness). The wind velocity profile retained was a prevailing wind direction towards 100° E (Fernandez-Turiel *et al*., 2019; Table S2). The grid data were introduced in the model, taking as reference the position of the volcano. Thus, the total area was a rectangle centred in the volcano (coordinates 0, 0) and defined by 100 km to W, 1000 km to E, and 300 km to N and S, respectively. The elevation should be equal for all points on the grid. An elevation of 1000 m was used as reference due to the large differences in elevation in the affected region. Grids of 5×5 km and 10×10 km were checked and the results were very similar. To reduce computing time the 10×10 km grid was retained for modelling. The configuration data for Tephra2 simulation are in Fernandez-Turiel *et al*., 2019; Table S3.

Results

On the basis of stratigraphy, geomorphology, physical volcanology, petrography, geochemistry, radiocarbon dating, and geographical distribution (Fig. 1b) of studied products we identified three main stratigraphic sequences: Cueros de Purulla, Cerro Blanco, and Bolsón de Fiambalá (Table 1).

Stratigraphy and description of deposits

The Cueros de Purulla sequence

The Cueros de Purulla (CdP) sequence consists of the lower CdP_1 and upper CdP_2 units (Table 1). The white CdP_1 unit mainly consists of fallout deposits, preserved in alluvial terrace and fan deposits that are elevated and isolated from active erosion channels (Figs. 3a and 3b). The CdP_1 unit is exposed up to several kilometres eastward from Cueros de Purulla volcano, with remnants recognised as far as 180 km from the probable vent. Proximal deposits consist of a series of 1-10 cm thick beds of lapilli and ash which together make up a total thickness between 20 and 70 cm. Some layers display normal grading of subangular pumice clasts, 1 to 60 mm in size. The content of lithic fragments is very low and includes exotic clasts of regional rocks that are generally smaller than 1 cm. Distal deposits of CdP_1 unit were recognized in the Tolombón–Cafayate area (Figs. 3a, 3b, and 4). The grain–size distribution of the ash is bimodal (Fig. 5a). The coarser and finer modes are 180 and 20 μm in the thin–bedded layers and 320 and 20 μm in the unstratified layers (Fig. 5a).

The unit CdP_2 includes two depositional sub–units (CdP_21 and CdP_22) that together filled 10 km of the valley located east of Cueros de Purulla volcano (Fig. 3c). The lower CdP_21 sub–unit is in direct contact with the CdP_1 unit. This contact is sharp and sometimes erosional. Internal stratification is lacking in both sub-units but reverse grading of pumice and normal grading of lithics occur occasionally. The pumice clasts are sub–rounded, ranging from 2 to 6 cm. The lithic fragments generally consist of angular to sub–angular country rocks ranging from 1 to 3 cm. These deposits show no evidence of welding or vesicle collapse.

The Cerro Blanco sequence

The Cerro Blanco sequence (CB) consists of at least seven sub–units, which we have grouped into three packages defined largely by observable unconformities (Fernandez-Turiel *et al.*, 2013, 2014, 2015) (Table 1).

The lowest unit CB_1 is exposed around the outer northern margin of the Cerro Blanco Caldera (Fig. 2), and is made up of angular decimetric rhyolitic blocks immersed in a rhyolitic lapilli and ash matrix with diffuse metre–scale stratification showing reverse grading. The deposits are clast–supported and some blocks exceed 1 m in size. There are not pumice clasts.

The CB_2 unit comprises three sub–units (Table 1). The lower CB_21 sub–unit mantled palaeotopography and is preserved as patches on hill slopes and above alluvial terrace deposits incised by active erosional channels (Fig. 3d). The thickness of these deposits ranges from 26 to 5 cm at distances of 11 to 200 km from the CBVC (Fig. 6). It consists in alternating, parallel, very thin beds of lapilli and ash (Fig. 7). The CB_22 sub–unit directly overlies CB_21. The contact is sharp and not erosional. It consists of an ash deposit without grading, with poorly defined stratification. CB_22 is locally overlain by alluvium or colluvium and elsewhere the surface has incipient soil developed on top (Figs. 7b, 7c, 7e, 7f and 7i).

The deposit thins from several meters near the vent to ~30 cm thickness at 170 km, but then thickens to > 300 cm thickness at ~200 km (Tafí del Valle area) before thinning once more at greater distances, e.g., ~20 cm thickness at

Table 1.—Stratigraphic summary of the studied volcanic sequences and their mineralogy.

Sequence	Unit	Sub-unit	Lithofacies and interpretation	Mineralogy
Bolsón de Fiambalá	BdF1		Alternating layers of moderate-poorly sorted, dacitic pumice lapilli and ash. Plinian fall deposit.	glass >> plagioclase, biotite, amphiboles, quartz >> magnetite, ilmenite, apatite, titanite
Cerro Blanco	CB_3 (postcaldera)	4	Alternating layers, 3-30 cm thick, of siliceous sinter. Deposits of hot springs.	amorphous silica
		3	Poorly defined decimetric-scale stratified deposits, poorly to very poorly sorted, with decimetric angular rhyolitic blocks in rhyolitic lapilli and coarse ash matrix deposits. Block-and-ash deposits.	glass >> feldspars, quartz, biotite, magnetite, ilmemite >> apatite, allanite-epidote, zircon
		2	Poorly to well–defined layers, 3-30 cm thick, white, rhyolitic lapilli and ash deposits. Fallout and phreatomagmatic deposits.	
		1	Crystal poor, very vesicular, rhyolite lava domes.	
	CB_2 (syncaldera)	3	Unstratified, matrix-supported, moderate to poorly sorted rhyolitic ignimbrite with clasts dominated by coarse pumice lapilli. Pyroclastic density current (PDC) deposits.	glass >> feldspars, quartz, biotite, magnetite, ilmenite > clinopyroxene, orthopyroxene, amphiboles > allanite-epidote, muscovite, titanite, zircon
		2	Unstratified rhyolitic ash. Plinian fall deposit.	
		1	Alternating layers, 1-3 cm thick, some of lapilli and some of ash. Rhyolitic Plinian fall deposit.	
	CB_1 (precaldera)		Poorly stratified lithic-rich breccia. Block-and-ash deposit.	glass >> feldspars, quartz, biotite, magnetite, ilmenite
Cueros de Purulla	CdP_2	1,2	Unstratified, matrix-supported, moderate to poorly sorted ignimbrite with clasts dominated by coarse pumice lapilli in $CdP_2$1 and lithic-rich $CdP_2$2. Pyroclastic density current (PDC) deposits.	glass >> feldspars, quartz, biotite, magnetite, ilmenite > apatite, allanite-epidote, muscovite, titanite, zircon
	CdP_1		Alternating layers, 1-10 cm thick, some of lapilli and some of ash. Rhyolitic Plinian fall deposit.	glass >> feldspars, quartz, biotite, magnetite, ilmenite > amphiboles, clinopyroxene > apatite, allanite-epidote, muscovite, titanite, zircon

370 km from the CBVC near Santiago del Estero (Figs. 6 and 7). As a first approach, an isopach map was constructed taking into account the field measurement of the fallout deposit thickness of $CB_2$2 (Fig. 8). To validate these isopachs, the calculated areas were examined in a semilog plot of the square root of the contour area versus isopach thickness (Fierstein & Hildreth, 1992; Fierstein & Nathenson, 1992; Hildreth & Fierstein, 2012a, 2012b; Pyle, 1989), testing three different models for tephra deposition (exponential, power–law, and Weibull) using the AshCalc code (Daggitt *et al.*, 2014). The lower mean relative squared error was obtained with the Weibull model (Fig. 8) (Fernandez-Turiel *et al*., 2019; Table S4).

These numerical approaches allow us to have a rough estimation of the volume of the Plinian deposits, despite the uncertainties owing to different features, e.g., thickness reduction by erosion of the upper part of deposits or error associated with techniques of estimating volume of fallout deposits by extrapolating thickness versus distance plots and assuming continuous decrease in thickness regardless of secondary thickening. The Weibull model provides a volume estimate of 172 km^3, higher than the power–law model (164 km^3) and lower than the exponential model (194 km^3) (Fernandez-Turiel *et al*., 2019; Table S2).

The particle size distributions of $CB_2$1 and $CB_2$2 are unimodal in proximal deposits and bimodal in distal deposits (>100 km from source) (Fig. 5b). In bimodal distributions, the lower size mode (~20 μm) does not change with distance (Fig. 5c). Instead, the upper size mode

Figure 3.—Three major rhyolitic eruptive events during Holocene time are represented by pyroclastic deposits studied in the southern Puna and neighbouring areas. Their geomorphological, stratigraphical, and sedimentological characteristics define three pyroclastic sequences. Cueros de Purulla sequence: (a) CdP_1 ash-fall layers a–d intercalated within alluvial fan deposits at the locality of Tolombón (section CB42; see also Fig. 4), (b) white CdP_1 ash-fall primary layer (4 m thick) elevated in a terrace in Cafayate (section CB43), and (c) $CdP_2$1 and $CdP_2$2 ignimbrites (section CB25). (d) The Plinian ash-fall deposit of Cerro Blanco unit in the cemetery of Tafí del Valle section ($CB_2$1 and $CB_2$2 sub–units; CB44 section; see also Fig. 4). (e) Detail of the BdF_1 ash-fall in Alto Las Juntas (CB111 section; see also Fig. 4). (f) The prehistorical settlement PB–NH3 of Palo Blanco discovered beneath a reworked BdF1 ash deposit.

shows a thinning from 600-700 to 100 µm particle size with distance up to ~200 km (Fig. 5c). Figure 5d shows the abundance of coarse and fine populations against distance for $CB_2$1 and $CB_2$2 sub–units. The coarse mode is less abundant with distance, but we cannot properly distinguish changes in volume of particles of finest mode (~20 µm) with distance.

The $CB_2$3 sub–unit filled the valleys north, northwest, and south of the CBVC and can be followed for more than 35 km. It directly overlies sub–unit $CB_2$1 in outcrops of

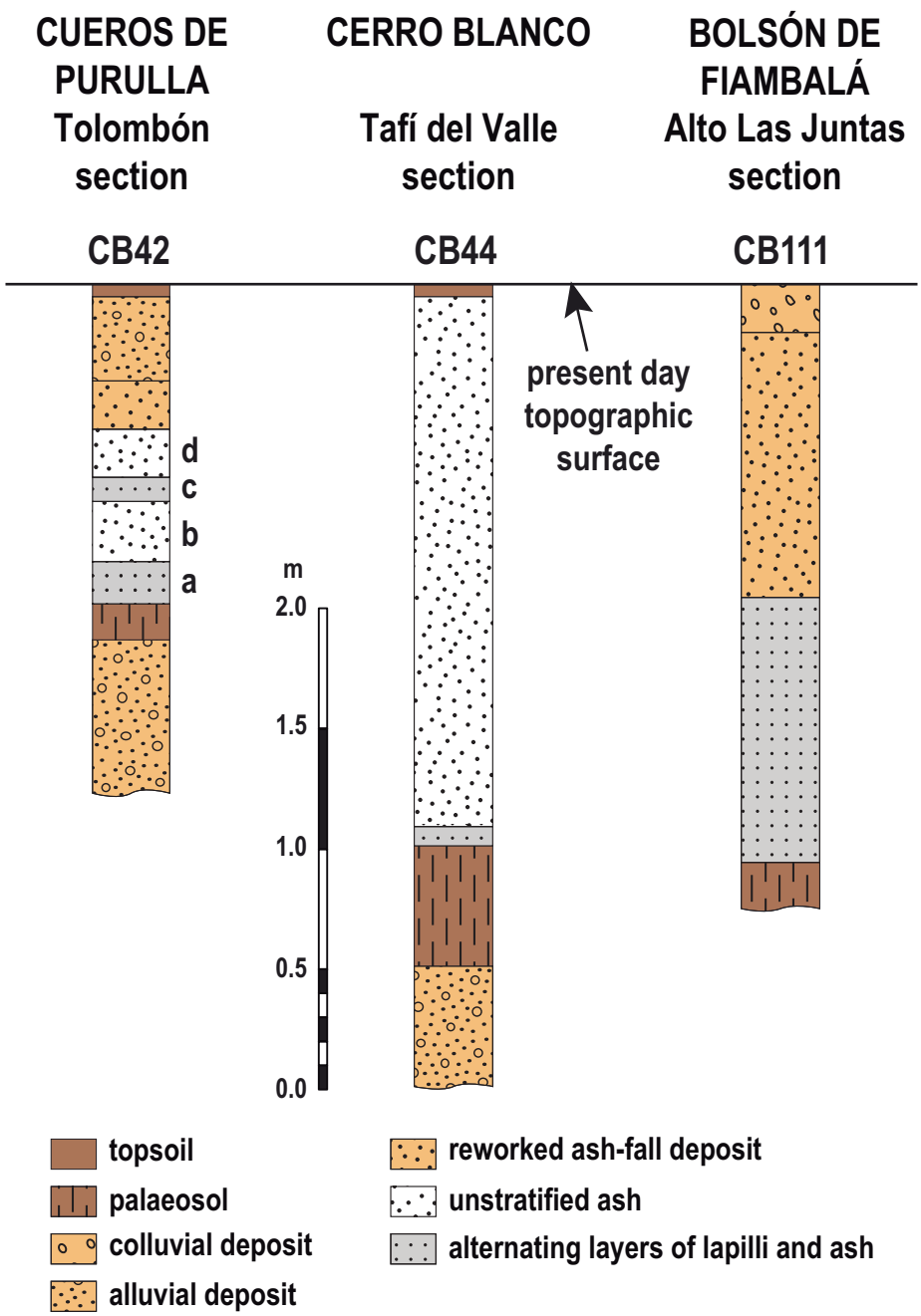

Fig. 4.—Key stratigraphic sections of the three major rhyolitic eruptive events recognized during Holocene in the southern Puna and neighbouring areas; Cueros de Purulla (picture in Fig. 3a), Cerro Blanco (see Fig. 3d) and Bolsón de Fiambalá units (see Fig. 3e).

the southern valleys with a sharp or, occasionally, erosive contact. The thickness reaches 30 m. Although strongly eroded, these deposits are well exposed in the valley of Las Papas (Figs. 1b, 9) where they are largely unstratified, homogeneous deposits with only locally developed, impersistent and diffuse layering of pumice and concentrated pumice lenses. The deposits are whitish, non–welded, and consist of poorly–sorted coarse pumice lapilli in a coarse ash matrix. Sub–rounded clasts of pumice are very abundant reaching ~20 cm in size. Sometimes the clasts show a subtle imbrication within the deposit. Sub–rounded to sub–angular exotic lithic clasts of local

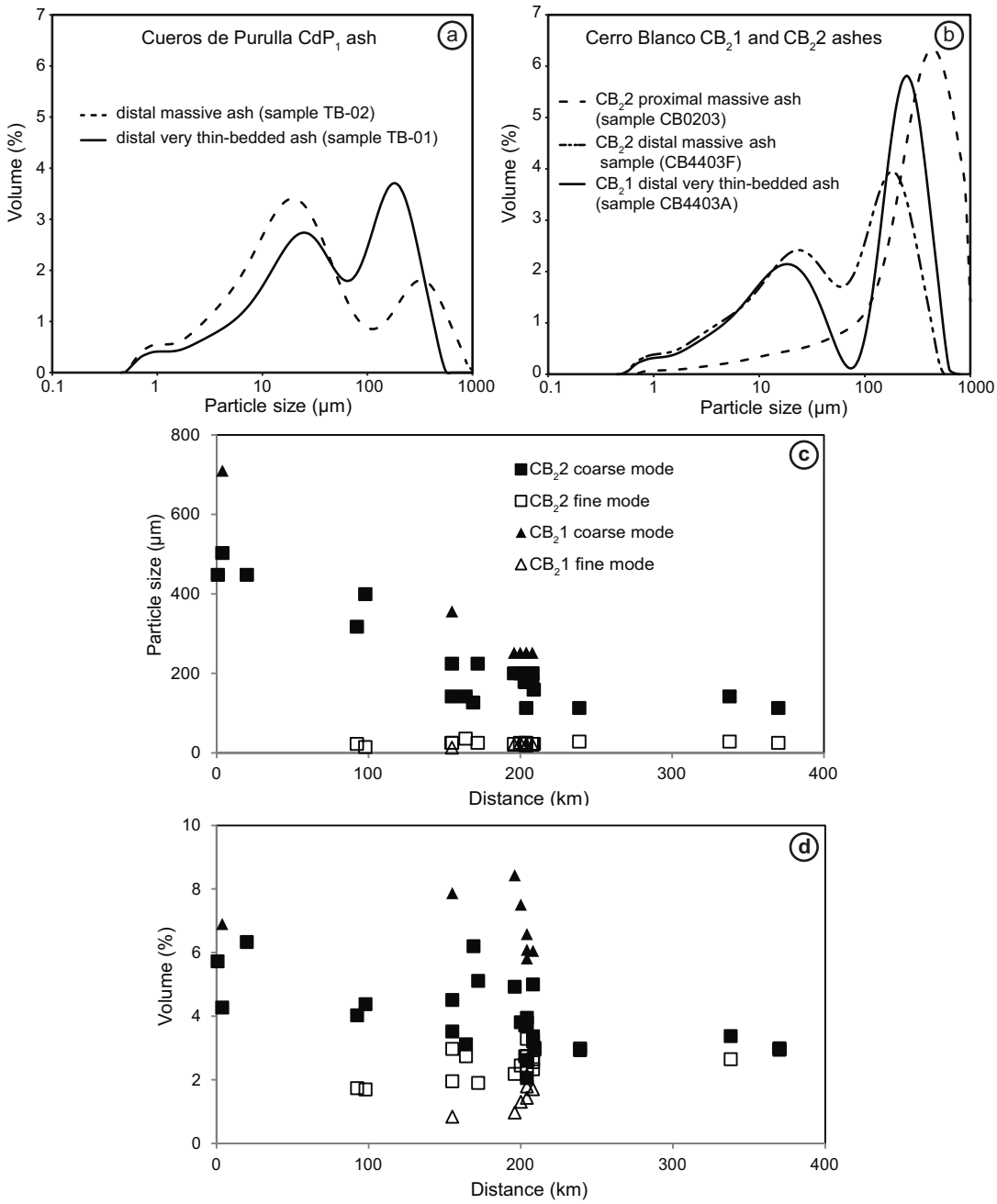

Fig. 5.—The particle size bimodality observed in primary distal CB and CdP deposits is interpreted as evidence of particle aggregation in the eruptive plume, forming cored ash clusters that typically break on impact with the ground. The resulting fallout deposit is made up of core particles of hundreds of microns in size and shell particles of tens of microns in diameter that covered the former. (a) Typical particle size distributions of volcanic ash of CdP_1 unit of Cueros de Purulla sequence, and (b) CB_21 and CB_22 sub–units of Cerro Blanco sequence. The particle size bimodality of Plinian ash-fall deposits is observed at >100 km from the CBVC: (c) Modes of unimodal and bimodal (coarse and fine) particle size distributions against distance for CB_21 and CB_22 sub–units of Cerro Blanco sequence; and (d) abundance of coarse and fine populations against distance for CB_21 and CB_22 sub–units of Cerro Blanco sequence.

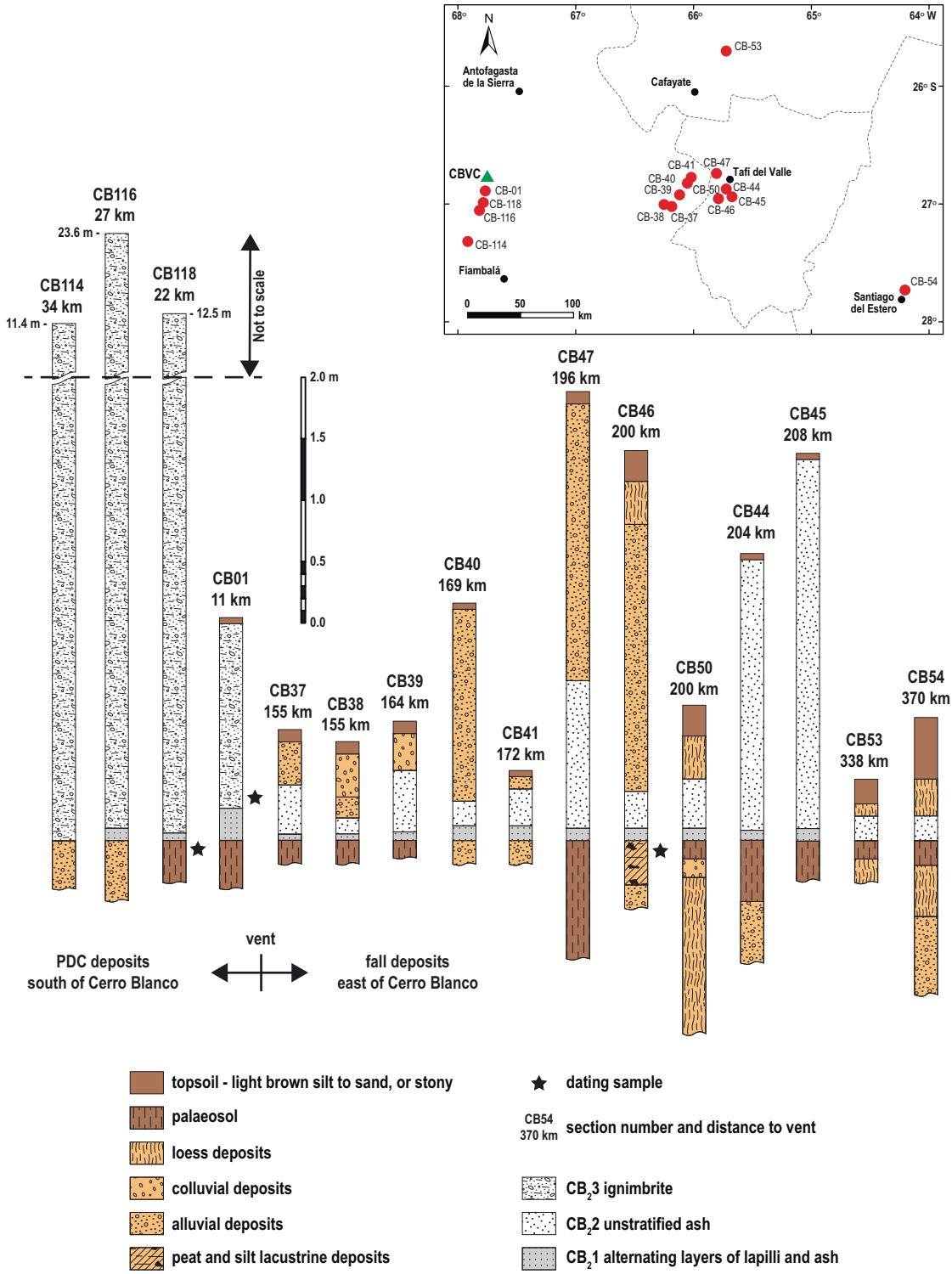

Fig. 6.—Stratigraphic sections of the Cerro Blanco sequence showing CB_2 deposits at different distances from the vent.

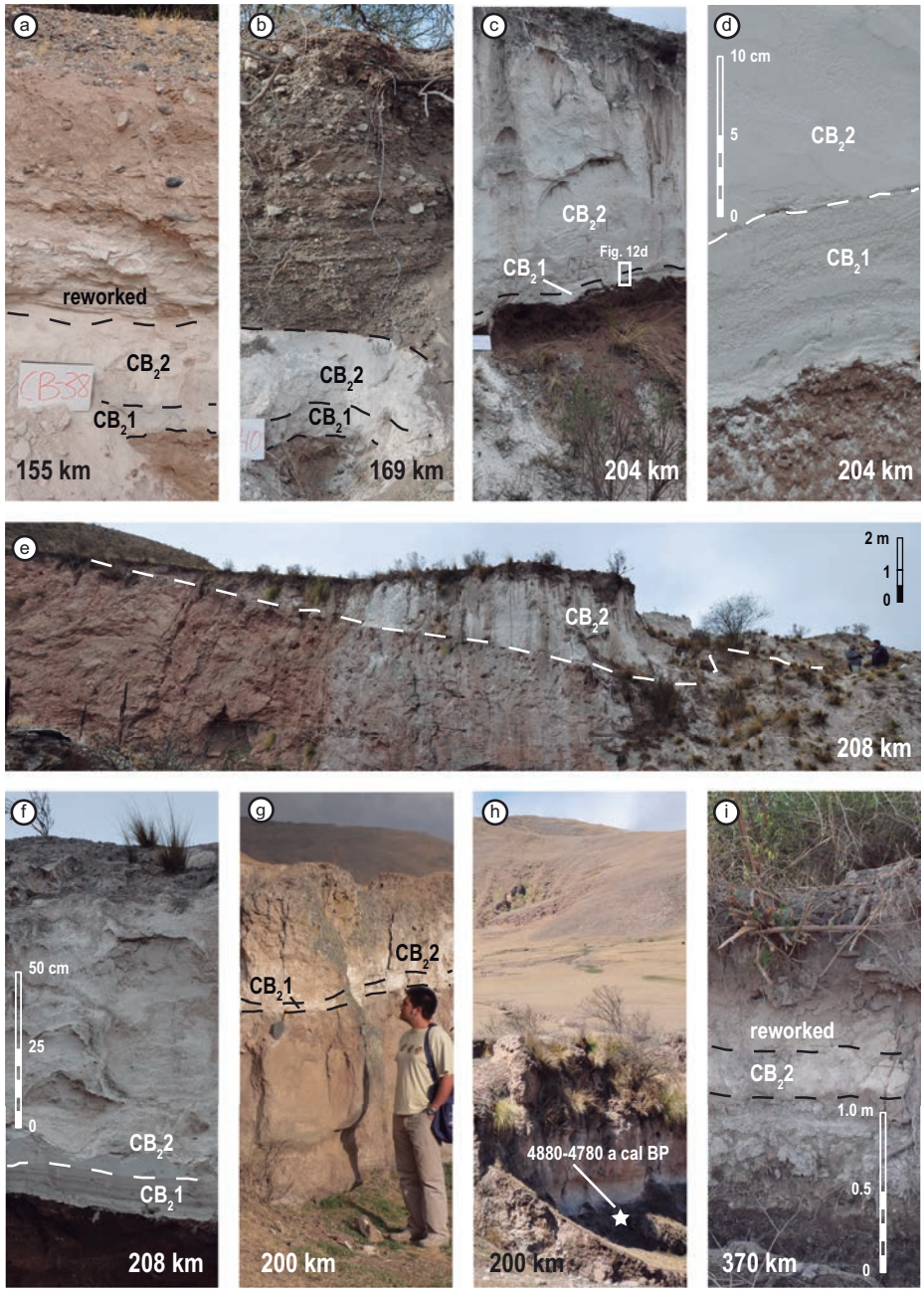

Fig. 7.—The first record of the Plinian column of the 4.2 ka cal BP Cerro Blanco eruption are a series of alternating layers, 1-3 cm thick, some of lapilli and some of ash ($CB_2$1 sub-unit). The change to the thicker, unstratified rhyolitic ash ($CB_2$2) indicates that the feeding system reached and maintained steady conditions during a single climactic column phase. This figure shows typical sections with distal Plinian $CB_2$1 and $CB_2$2 fall ash deposits, from 155 to 270 km east of Cerro Blanco. (a) Primary Plinian fall ash of CB_2 deposits covered by reworked ash and alluvial deposits (CB38 section). (b) $CB_2$1 and $CB_2$2 fall ash deposits intercalated within alluvial deposits (CB40 section). (c) Plinian fall ash layers of CB_2 resting on organic-rich soil, the ash deposit has incipient soil developed on top (CB44), and (d) detail where the alternating fall layers of $CB_2$1, some of lapilli and some of ash and the unstratified ash-fall of $CB_2$2 are observed above palaeosol. (e) General view of Plinian fall ash CB_2 deposits at Zanja del Chivo, Tafí del Valle area (CB45 section), and (f) detail of lower alternating fall layers of $CB_2$1 and the upper unstratified fall deposits of $CB_2$2. (g) CB_2 ash-fall deposits overlain by loess (section CB50). (h) Intercalated CB_2 ash-fall deposits in lacustrine sediments; peat dated 4880-4780 a cal BP is overlain by the Cerro Blanco ash deposit (section CB46). (i) The most distal studied section where only the $CB_2$2 fall ash deposit is observed (section CB54). Sample number card is 10.5 × 14.7 cm.

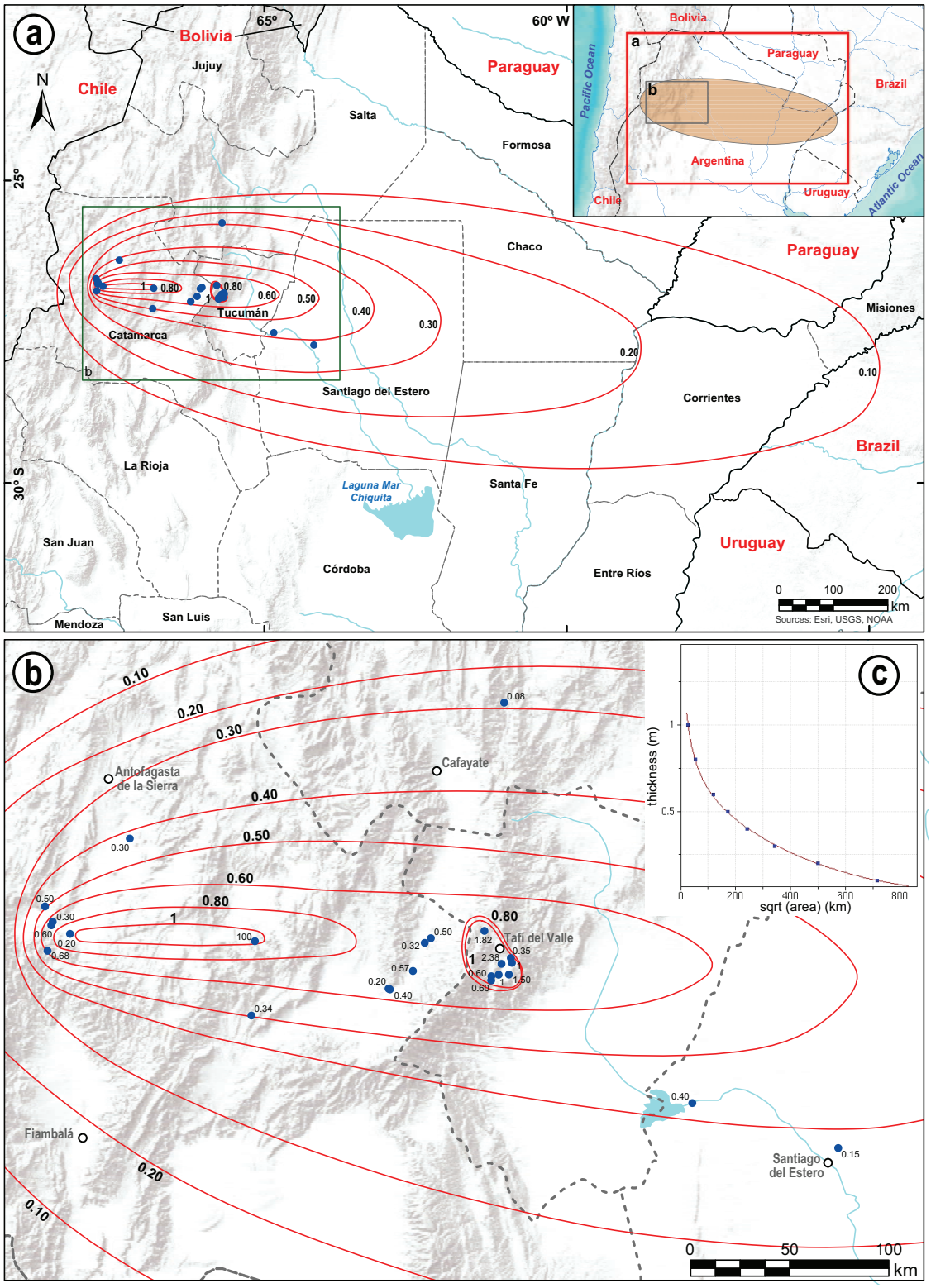

Fig 8.—Isopach maps (m) for the $CB_2$1 and $CB_2$2 fall deposits of Cerro Blanco Volcanic Complex, (a) showing up to the inferred area of 0.10 m isopach, and (b) in the sampled area indicating the measured thickness. (c) Semi–log plot of thickness vs. $(area)^{1/2}$ shows the best fit model (Weibull) for isopach adjustment.

metamorphic and volcanic rocks, 1–20 cm in diameter, are abundant at the basis of the unit in many places. Parallel and cross bedded, 0.2 to 2 m thick beds occurs particularly on palaeotopographic highs.

The unit CB_3 consists of four sub–units (Table 1), all of them exposed close or within the caldera of Cerro Blanco. The exceptional preservation of these sub–units is mostly due to the arid environment of the region (Aulinas *et al.*, 2015). The $CB_3$1 sub–unit comprises crystal poor, very vesicular, rhyolite lava domes. These domes were described in detail by Báez *et al.* (2016). The largest dome appears in a rectangular shape of 2.7 × 1.4 km, and cut the SW caldera margin. In addition, three other smaller, pinkish, extra–caldera domes are aligned along a trend N100°E that includes the above–mentioned larger dome. The largest dome cut the caldera margin, indicating their post–caldera emplacement and a change in the eruptive style from highly explosive to effusive–moderately explosive.

The $CB_3$2 sub-unit is made up of 3-30 cm thick, white lapilli and ash deposits organized in poorly to well–defined layers (Fig. 2a), forming the highest peaks of the CBVC, surpassing 4700 m a.s.l.; lava blocks are common within the deposit and, in some cases, show

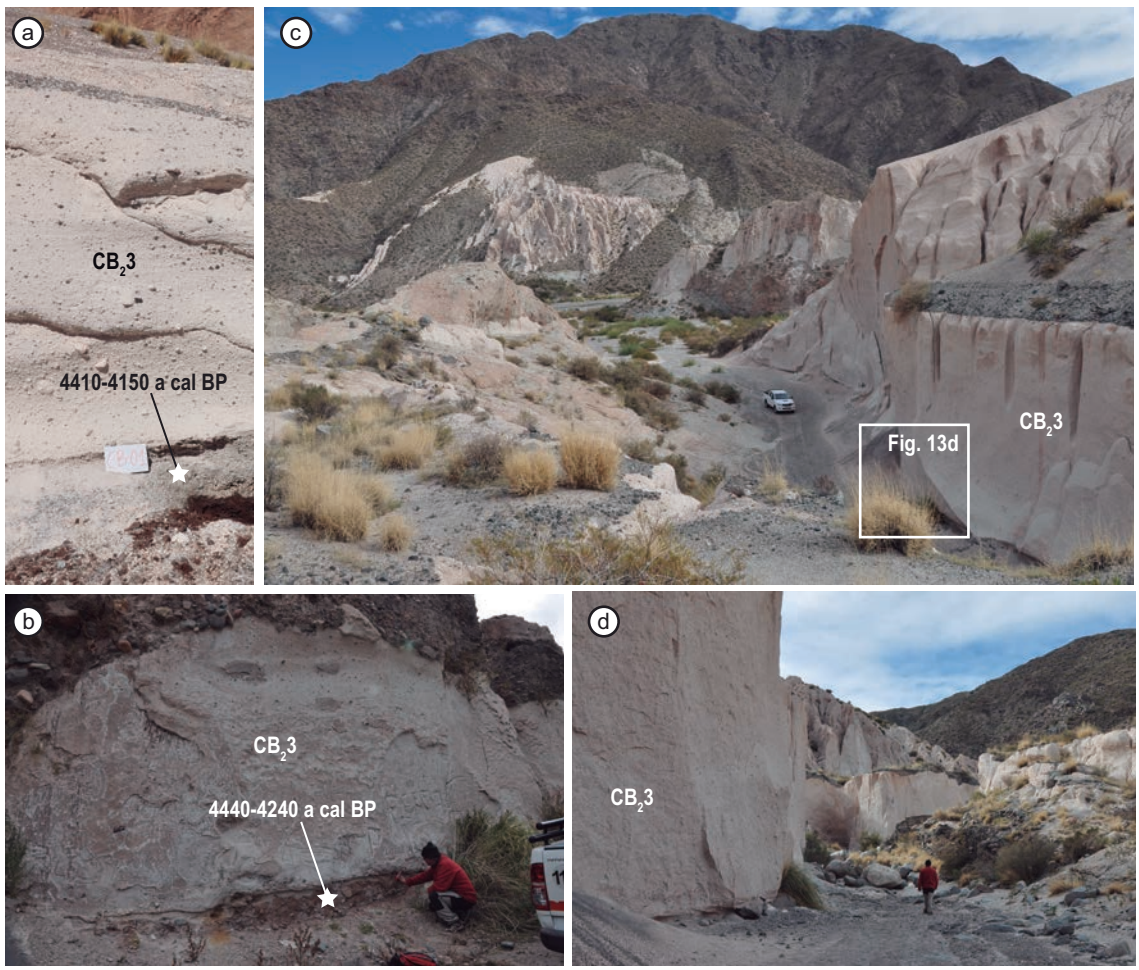

Fig. 9.—$CB_2$3 ignimbrite in different places of Las Papas Valley. (a) Vaguely stratified, matrix-supported, 1.5 m thick, moderate to poorly sorted rhyolitic ignimbrite with clasts dominated by coarse pumice lapilli, Laguna Aguada Alumbrera, section CB01, 11 km from vent; sample number card is 10.5 × 14.7 cm. Charred material within the lower part of the ignimbrite provided an age of 4410-4150 a cal BP. (b) Unstratified, matrix-supported, 10 m thick, moderate to poorly sorted rhyolitic ignimbrite with clasts dominated by coarse pumice lapilli, Section CB118, 22 km from vent. Charred material within soil beneath the ignimbrite was dated 4440-4240 a cal BP. (c-d) Exceptional exposure, ~30 m high, of unstratified nonwelded ignimbrite $CB_2$3, 27 km south from vent, base rests on fluvial deposits, Section CB 116.

a bread crust structure. The thickness reaches 150 m. These deposits are around the main lava dome, except on the side oriented towards the caldera centre where the lava dome is directly in contact with $CB_3$3. These deposits are interpreted as fallout from eruptions associated with these structures (Báez *et al.*, 2016). Within the unit also phreatomagmatic deposits with lapilli and ash can be observed, characterized by low–angle cross stratification.

The deposits of $CB_3$3 form several overlapping lobes reaching ~3.5 km from the main lava dome to the opposite wall of the caldera (Fig. 2), almost completely covering the bottom of the Cerro Blanco Caldera. They consist of 10-100 cm thick beds, diffusely stratified, and made up of decimetric angular blocks of pumice immersed in a coarse lapilli matrix. The total thickness reaches up to 50 m.

The Cerro Blanco sequence ends with 1–5 m thick deposits of siliceous sinter in the middle of the caldera ($CB_3$4).

The Bolsón de Fiambalá sequence

A third sequence is defined on basis of the geomorphological, stratigraphical, mineralogical, and chemical characteristics of numerous outcrops occurring in the northwest of Bolsón de Fiambalá (BdF), 40–60 km to the south of CBVC (Fig. 1). We combine these deposits in only one lithostratigraphic unit called BdF_1 (Table 1). It mantles the palaeotopography with a series of unstratified and diffusely parallel medium bedded layers which together make a total thickness between 0.8 and 1.6 m. Some layers are pumice lapilli and others are largely ash. Occasionally, layering is highlighted by alignments of pumice of ~1 cm in size. BdF_1 is locally overlain by alluvium or hillslope colluvium, but also by aeolian deposits of lapilli and ash.

Compositional characteristics

The Cueros de Purulla sequence

The ash of the CdP_1 unit in the Cueros de Purulla sequence is made up of glass shards and micropumices, with angular to sub–angular blocky shapes containing tubular vesicles (Fernandez-Turiel *et al*., 2019; Fig. S1). The dominant phenocrysts are biotite, which is the distinguishing feature of these deposits in the field, feldspars (plagioclase >> K–feldspar), quartz, titanomagnetite, and ilmenite. Amphiboles and clinopyroxenes are minor contents. Apatite, allanite–epidote, muscovite, titanite and zircon can be found in trace amounts.

The ash-dominant matrix in the CdP_2 unit is fine to coarse in size and consists of pumiceous glass shards, and very abundant feldspar (plagioclase >> K–feldspar), biotite, and quartz crystal fragments (Fernandez-Turiel *et al*., 2019; Fig. S1).

The glass compositions of the CdP units are rhyolitic (74.8–79.2 wt% SiO_2; 5.8–10.8 wt% Na_2O+K_2O) (Fig. 10). Feldspars are dominated by plagioclase (Fig. 11). In the different plagioclases, the anorthite (An) decreases from 41.7 to 23.4 mol %, with an increase in orthoclase (Or) from 2.8 to 6.6 mol % (n = 80). The Or content of K–feldspar ranges from 69.5 to 71.3 mol %, with an An < 1.2 mol % (n = 11).

Biotite typically contains 36.9 ±0.8 wt% SiO_2 (mean ±1 standard deviation), 13.7 ±0.3 wt% Al_2O_3, and has a Mg number Mg# = (100 × [mol Mg] / [mol Mg + Fe]) of 59 ±1. The TiO_2 content is 5.0 ±0.2 wt%, and the MnO content is 0.35 ±0.03 wt% (Fig. 12).

Titanomagnetite is more common than ilmenite. The TiO_2 content ranges 5–7 wt% and MnO is ~1 wt% in titanomagnetite, while ilmenite contains ~35 wt% TiO_2 and ~1 wt% MnO (Fig. 13).

The rare clinopyroxene found in the CdP_1 unit (n = 5) are diopsides (Fig. 14). Amphibole crystals are also rare in the Cueros de Purulla sequence and were only observed in CdP_1 unit (Fig. 14). Compositions include magnesiohornblende and pargasite, according the IMA 2012 recommendations (Locock, 2014). These samples showed values of Al# exceeding 0.21, the threshold at which the amphiboles are inferred to represent xenocrysts of crustal or mantle materials (Ridolfi *et al.*, 2010).

The Cerro Blanco sequence

The products of Cerro Blanco sequence showed a large homogeneity in composition, mineralogically and chemically. For example, both $CB_2$1 and $CB_2$2 ash sub–units are mainly composed of cuspate and blocky glass shards (~90%), but also contain feldspars (~5%), quartz (~3%), and biotite (< 2%), often as free crystals (Fernandez-Turiel *et al*., 2019; Figs. S1 and S2). Minor contents include magnetite, ilmenite, clinopyroxene, orthopyroxene, amphiboles, allanite–epidote, muscovite, titanite, and zircon. Lithic fragments are very rare.

The lava domes and the deposits of $CB_3$2 and $CB_3$3 are porphyritic and very vesicular; their glassy matrices

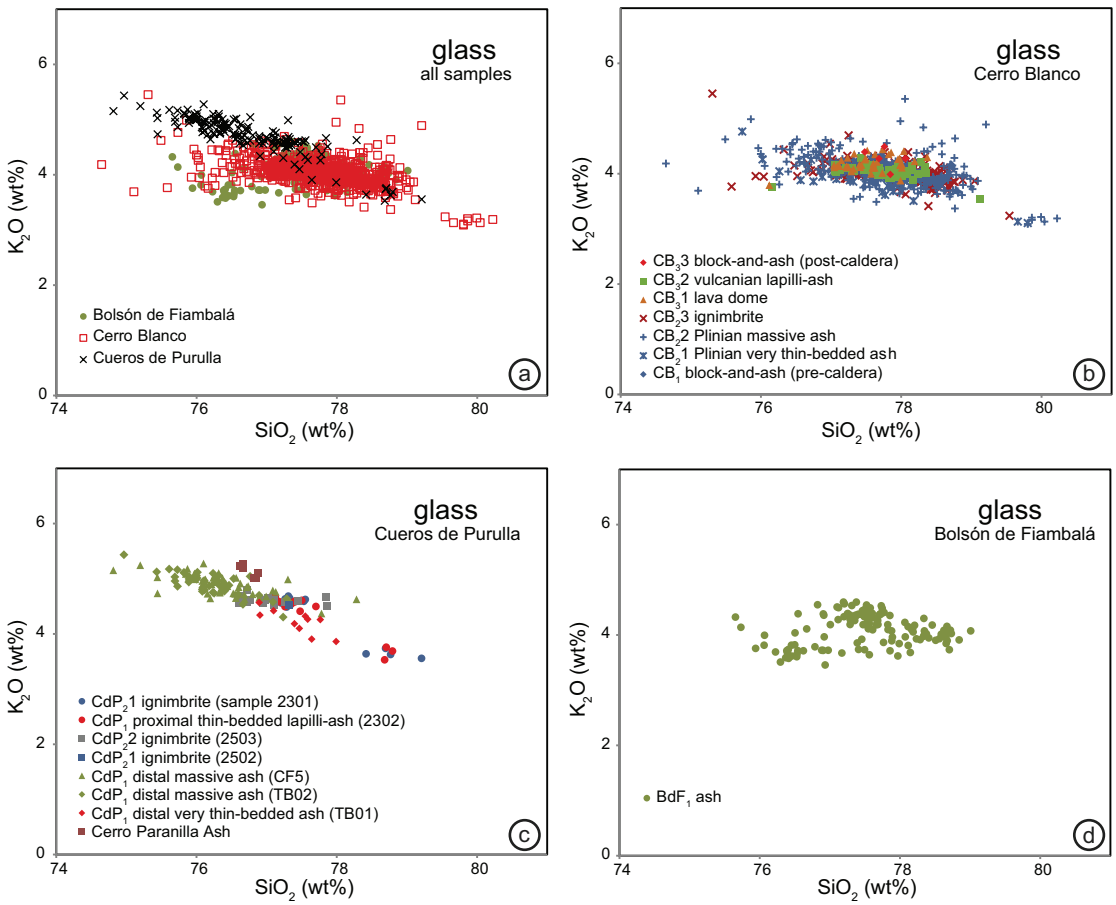

Fig. 10.—SiO_2–K_2O diagrams: (a) glass analyses normalized to 100% of Cueros de Purulla, Cerro Blanco, and Bolsón de Fiambalá sequences. For clarity, glass analyses shown separately for (b) Cerro Blanco, (c) Cueros de Purulla, (d) Bolsón de Fiambalá. Compositional data of glass and minerals (Figs. 10-14) and the unique occurrence of abundant large biotite crystals visible to the naked eye assist the association of the fallout deposits of Tolombón and Cafayate (CdP_1 unit) with the published Cerro Paranilla Ash (Hermanns *et al.*, 2000).

include quartz and alkali feldspars as the main phenocrysts, and biotite and Fe–Ti oxides as minor phases. There are also rare apatite, allanite–epidote, and zircon phenocrysts. A detailed description of lava domes was perfomed by Báez *et al.*, 2016.

The glass composition of all CB units is rhyolitic (74.6–80.2 wt% SiO_2, normalized to anhydrous contents) with alkali concentrations of 3.1–5.4 wt% K_2O (Fig. 10), 2.1–6.2 wt% Na_2O, and CaO < 0.9 wt%.

In the CB sequence, K–feldspar is more abundant than plagioclase and, while two groups of plagioclases are observed, only one group of K–feldspars can be distinguished (Fig. 11). Both groups of plagioclases coexist in the same sample. In one group of plagioclases, the An content in different crystals decreases from 44.3 to 28.5 mol %, with an increase in Or content from 2.3 to 8.1 mol % (n = 16). On the other hand, the second group shows An content in different crystals decreasing from 19.5 to 10.2 mol %, with an increase in Or content from 4.5 to 7.2 mol % (n = 138). The Or content in different crystals of K–feldspar ranges from 61.6 to 72.5 mol %, with an An content of < 1.3 mol % (n = 259).

The TiO_2–MnO diagram of biotite provides a good chemical discrimination between two groups of biotites of the CB sequence: a high–MnO (1.11 ±0.06 wt%) and a low–TiO_2 (3.5 ±0.2 wt%) group and a low–MnO (0.21 ±0.07 wt%) and high–TiO_2 (4.7 ±0.7 wt%) group (Fig. 12). Both groups can be observed in the same sample.

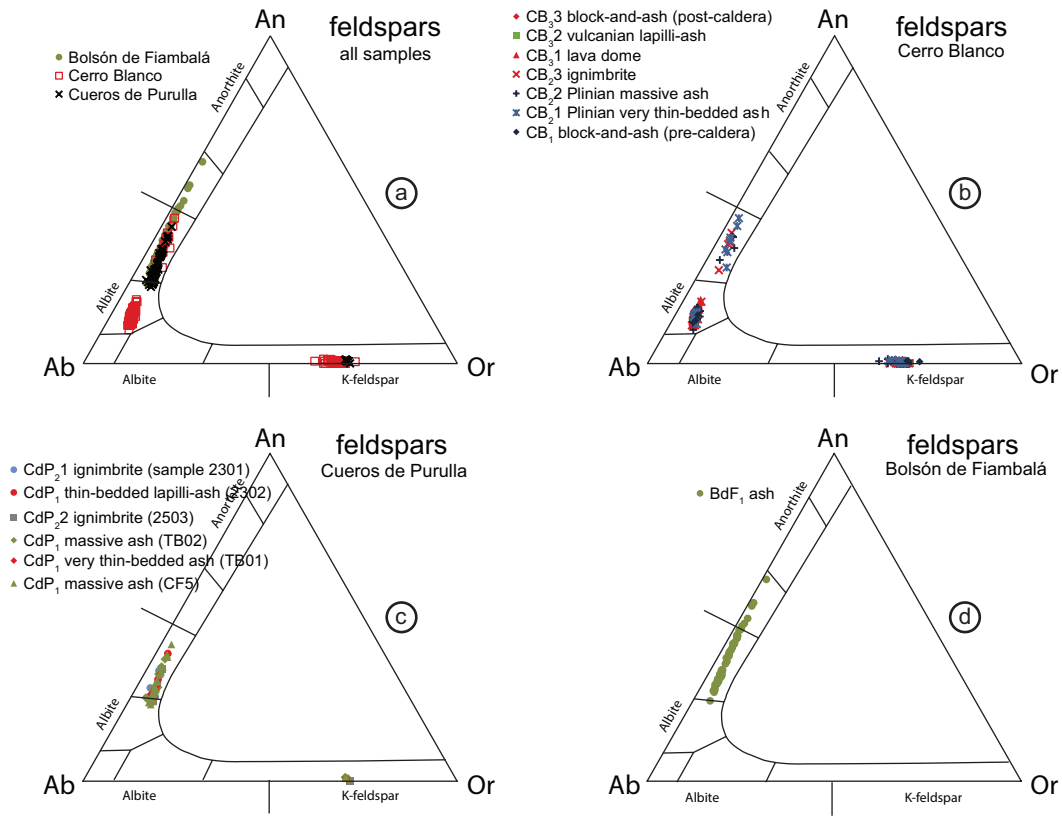

Fig. 11.—Anorthite–albite–orthoclase (An–Ab–Or, mol %) ternary diagrams showing the compositions of feldspars of Bolsón de Fiambalá, Cerro Blanco, and Cueros de Purulla sequences, (a) for all samples and, for clarity, (b-d) shown separately for units and sub–units of Cerro Blanco, Cueros de Purulla, and Bolsón de Fiambalá.

The rest of the major elements show similar concentrations in both groups. The high–MnO group is relatively compact and includes samples from all sub–units of the CB sequence. However, the low–MnO group of biotites occurs only in CB_2.

The CB sequence contains two distinct titanomagnetite and ilmenite populations. Examples of both groups coexist in the same sample and exsolution features are not observed within the grains. One group is compositionally compact, showing minimal variability among CB sub–units with a TiO_2 content 2.6–3.7 wt% and MnO 2.4–3.2 wt% in titanomagnetite, and 41.3–45.4 wt% TiO_2, and 4.7–7.9%, m/m MnO in ilmenite (Fig. 13). The other group was found only in the three sub–units of the CB_2 unit, i.e., those related to the paroxysmal phase, and it contains lower concentrations of MnO in both titanomagnetite (0.3–1.9 wt% MnO) and ilmenite (0.3–0.7 wt% MnO), and wide ranges of TiO_2 in titanomagnetite (1.5–8.2 wt%) and in ilmenite (0.3–0.7 wt%). The abundance ratio of titanomagnetite/ilmenite is ~50/50 in the high–Mn group, while the titanomagnetite dominates ilmenite in the low–Mn group.

The rare clinopyroxene and orthopyroxene in the CB sequence (n = 9) were found in sub–units CB_21, CB_22, and CB_23. They have a greater compositional variability than the pyroxenes of the CdP_1 unit (Fig. 14). They were not in equilibrium with melt, being probably xenocrystic. Amphibole crystals are found only in the CB_2 unit. Compositions include magnesio–ferri–hornblende, magnesio–hastingsite, and pargasite, following IMA 2012 recommendations (Locock, 2014) (Fig. 14).

The Bolsón de Fiambalá sequence

The tephra deposits of BdF sequence are crystal–poor and lithic–poor made up of pumice, glass (subangular blocky shards) (~50%), amphiboles (~5%), plagioclase

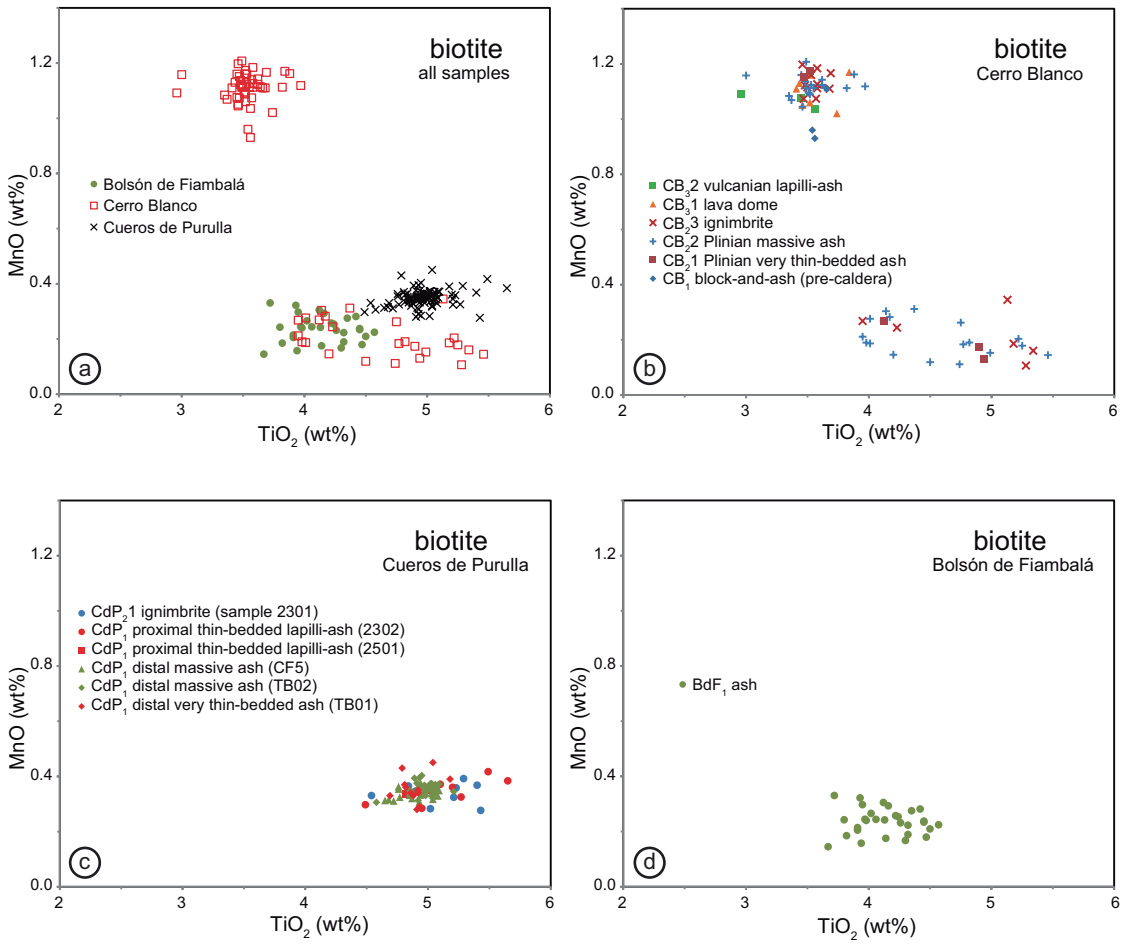

Fig. 12.—TiO_2–MnO compositions of biotites of Bolsón de Fiambalá, Cerro Blanco, and Cueros de Purulla sequences, (a) for all samples and, for clarity, (b-d) shown separately for units and sub–units of Cerro Blanco, Cueros de Purulla, and Bolsón de Fiambalá.

(~35%), biotite (~3%), and quartz (~5%); magnetite, ilmenite, apatite, and titanite are scarce (2-3%). We did not find pyroxene in the BdF sequence.

The glass compositions of BdF_1, with values normalized to anhydrous compositions, are rhyolitic (75.6–79.0 wt% SiO_2, with alkali concentrations of 3.5-4.6 wt% K_2O, 3.1-4.3 wt% Na_2O, and 1.0-2.1 wt% CaO) (Fig. 10). In different crystals, the An content of plagioclase of the BdF sequence decreases from 61.5 to 24.5 mol %, with an increase in Or content from 1.1 to 6.6 mol % (n = 65) (Fig. 11). The biotite of the BdF sequence typically contains 37.4 ±0.7 wt% SiO_2 (mean ±1 standard deviation), 13.7 ±0.2 wt% Al_2O_3, and have a Mg number (100 × [mol Mg] / [mol Mg + Fe]) of 59 ±2. TiO_2 content is 4.1 ±0.2 wt% and MnO is 0.24 ±0.05 wt% (Fig. 12). Unfortunately, Fe–oxides were not analysed in this sequence.

Compositions of amphibole phenocrysts of the BdF sequence include magnesio–ferri–hornblende, magnesio–hastingsite, Ti–rich magnesio–hastingsite, and magnesio–hastingsite, according the IMA 2012 recommendations (Locock, 2014). Their A–C variation is close to the CB sequence and quite different from the CdP sequence (Fig. 14).

Geothermobarometry

The Cueros de Purulla sequence

Feldspar data were used to estimate the temperature. Three pairs of alkali feldspar–plagioclase crystals from CdP_1, using the two–feldspar thermometer (eqn. 27b, Putirka 2008), yield temperatures between 780 and 800 °C for 5 kb.

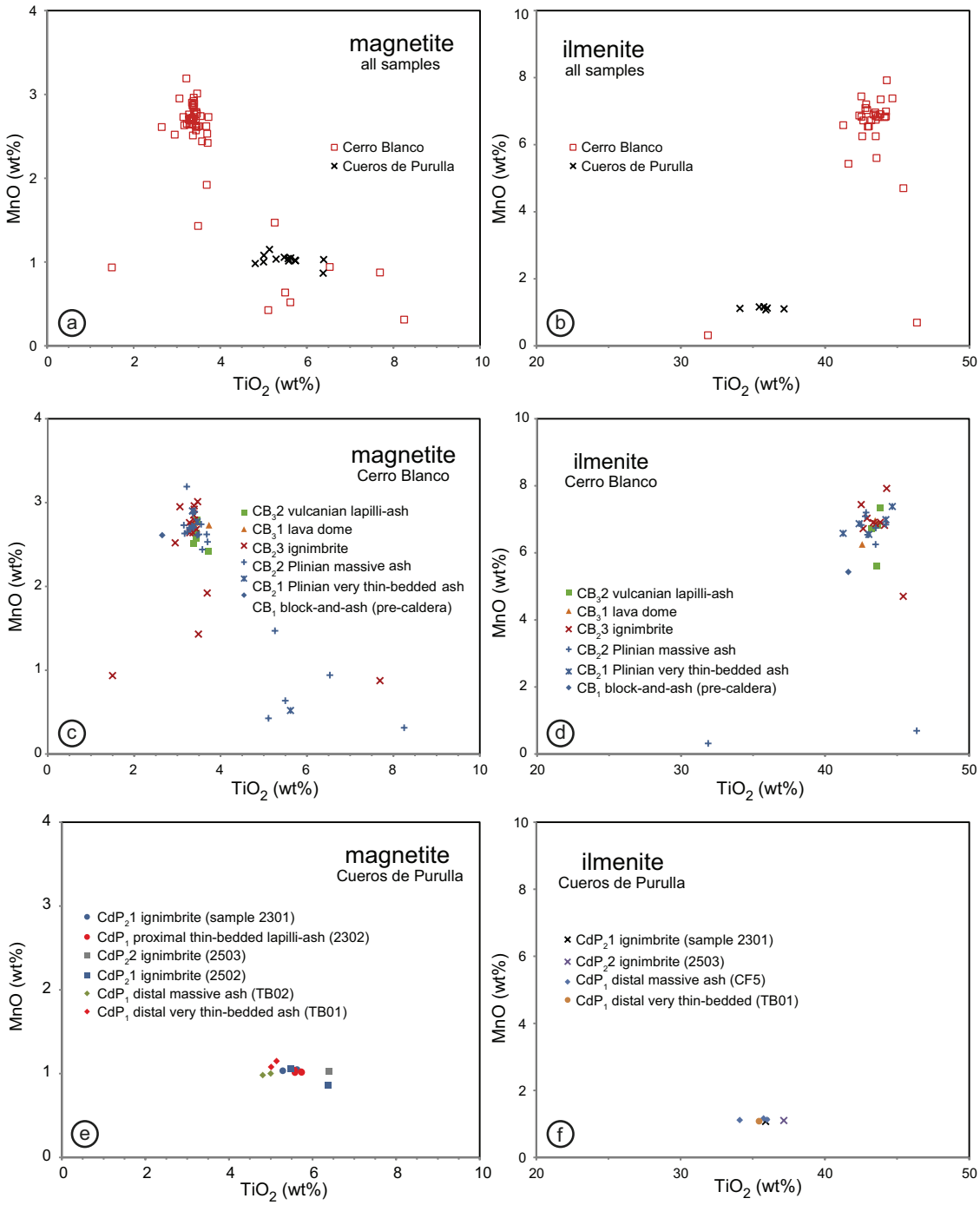

Fig. 13.—TiO_2–MnO compositions of Fe–Ti oxides of Cerro Blanco, and Cueros de Purulla sequences, (a-b) for all samples and, for clarity, (c-f) shown separately for their units and sub–units.

Coexisting titanomagnetite–ilmenite pairs were evidenced in three samples, one each from CdP_1, $CdP_2$1, and $CdP_2$2. Fe–Ti exchange temperatures, calculated using the Fe–Ti two oxide geothermometer and oxygen–barometer (Ghiorso & Evans, 2008), fall in the range of 750 to 800 °C. Results are also indicative of oxidizing conditions (log fO_2 relative to NNO between 1.2 and 1.4) and elevated TiO_2 activity (a_{TiO2} ~0.8) in the magma just prior to eruptive quenching.

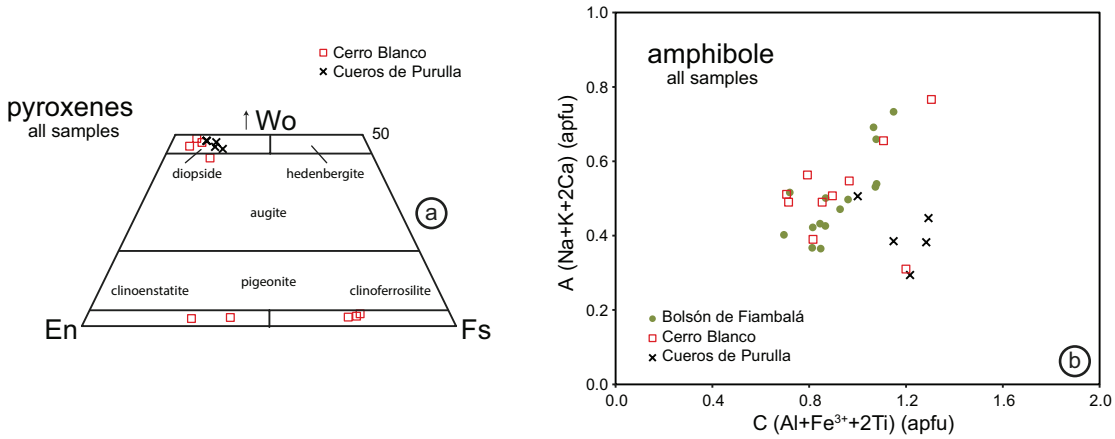

Fig. 14.—(a) Wollastonite–enstatite–ferrosilite (Wo–En–Fs, mol %) diagram of pyroxenes. (b) C–A diagram of amphiboles of Bolsón de Fiambalá, Cerro Blanco, and Cueros de Purulla sequences.

The diopsides of CdP_1 unit allowed the use of the equilibrium pairs of clinopyroxenes and melt to determine both temperature and pressure conditions (eqn. 35 for T and eqn. 30 for P, Putirka, 2008). For melt composition, we used average glass composition of samples with clinopyroxene. Mineral–melt pairs were checked to ensure they satisfy the equilibrium condition $K_D(Mg–Fe)^{cpx–liq}$ = 0.28 ±0.08 (eqn. 35, Putirka, 2008) (Gilbert *et al.*, 2014; Schindlbeck *et al.*, 2014). Clinopyroxene–liquid pairs satisfying the before–mentioned equilibrium condition (n = 5) yielded a temperature of 795–828 °C and a pressure of 3.7–8.3 kb with $0.21 < K_D(Mg–Fe)^{cpx–liq} < 0.23$.

The Cerro Blanco sequence

Pre–eruption conditions were constrained using the chemistry of feldspars (Putirka, 2008), Fe–Ti oxides (Ghiorso & Evans, 2008), and amphibole (Ridolfi *et al.*, 2010). Twenty pairs of alkali feldspar–plagioclase from CB_1, CB_2, and CB_3 provided temperatures between 610 and 700 °C (modelled at 1 kb) for plagioclase with $An_{10–20}$, and four pairs of $CB_2$1 and $CB_2$2 sub–units resulted in 750 to 810 °C (modelled at 1 kb) for plagioclase with $An_{28–44}$.

Fe–Ti oxides in CB_1 (n=1 pair) yielded an equilibration temperature of ~590 °C and a log fO_2 value of 1.2 (relative to NNO). CB_2 pairs (n = 10) provided from 580 to 725 °C and log fO_2 of 0.4–0.9. Only one pair of low–MnO titanomagnetite–ilmenite was found and it showed 794 °C and log fO_2 of 1.3. Finally, $CB_3$3 pairs (n = 3) indicated ~610–630 °C and log fO_2 of 0.7–0.8.

Physical–chemical conditions during amphibole formation were estimated by applying the thermobarometric method based on Al contents resulting in temperatures from 801 ±22 to 1009 ±22 °C, pressures from 108 ±12 to 554 ±61 MPa, water contents of the melt from 3.8 ±0.4 to 7.6 ±0.4 wt%, and log $f(O_2)$ from -8.8 ±0.4 to -12.8 ±0.4. The reliability of this thermobarometer was discussed (Erdmann *et al.*, 2014; Ridolfi & Renzulli, 2012), showing incorrect pressure values but reasonable estimations of temperature and oxygen fugacity (Pignatelli *et al.*, 2016). These higher temperatures in comparison with feldspars and Fe-Ti oxides possibly indicate that these crystals are xenocrysts.

The Bolsón de Fiambalá sequence

Applying the thermobarometric method for amphibole phenocrysts of the BdF sequence (Ridolfi *et al.*, 2010) yielded temperatures from 793 ±22 to 950 ±22 °C, pressures from 94 ±10 to 317 ±35 MPa, water contents of the melt from 4.1 ±0.4 to 5.3 ±0.8 wt%, and log $f(O_2)$ from –10.4 ±0.4 to –12.4 ±0.4. The pressure values could be incorrect according to discussions on this thermobarometer (Erdmann *et al.*, 2014; Pignatelli *et al.*, 2016; Ridolfi & Renzulli, 2012).

Radiocarbon dating

Three new radiocarbon ages were obtained for CB sequence (Fernandez-Turiel *et al.*, 2014). A peat beneath $CB_1$1 unit at Tafi del Valle area (Arroyo Las Perillas, El

Rincón) yielded a radiocarbon age of 4880–4780 a cal BP (Fig. 7h; Fernandez-Turiel *et al*., 2019; Table S1). In addition, charred material trapped inside $CB_1$3 near Laguna Aguada Alumbrera indicated an age of 4410–4150 a cal BP (Fig. 9a; Fernandez-Turiel *et al*., 2019; Table S1). This age is consistent with that obtained from charred vegetation in a palaeosol underneath this ignimbrite at Las Papas: 4440–4240 a cal BP (Fig. 9c; Fernandez-Turiel *et al*., 2019; Table S1).

Eruption modelling of CB2 deposits

Tephra2 simulation results for CB_2 deposits indicates that tephra fall deposit was mainly distributed towards ESE (Fernandez-Turiel *et al*., 2019; Fig. S3). These results are compatible with the geographical ellipticity of the CB_2 deposits (Fig. 8), caused by the paroxysmal phase of 4.2 ka cal BP eruption of CBVC, strongly suggesting windy atmospheric conditions at the time of the eruption with a general dispersion towards the ESE. The simulation showed 0.5 m isopach contour reached as far as 400 km from the source (near Santiago del Estero). The preserved thickness in this area reaches 0.2-0.4 m (Figs. 6 and 7 i). The estimated plume height of the eruption was 27 km. The plume ratio of 0.9 indicated that pyroclastics were released from the upper 10% of the eruption column.

Discussion

Volcanic meaning of studied sequences

The Cueros de Purulla sequence

The CdP_1 unit is interpreted as air-fallout deposits from the buoyant eruption plume of a highly explosive eruption (Cas & Wright, 1988). The mineralogical and chemical correlation of proximal and distal deposits showed that ash-fall reached more than 180 km eastward Cueros de Purulla volcano (CdP). Reworking is discarded as the origin of grain–size bimodality, because this feature is observed in primary deposits. This bimodality is interpreted as evidence of aggregation of particles in the eruption cloud (Bagheri *et al.*, 2016; Brazier *et al.*, 1983; Brown *et al.*, 2012; Sorem, 1982). The CdP_2 deposits are interpreted as ignimbrites emplaced in successive eruptive pulses.

The Cerro Blanco sequence

The Cerro Blanco sequence (CB) was interpreted largely by observable unconformities that developed in response to caldera collapse during the evolution of the Cerro Blanco Volcanic Complex (CBVC) (Báez *et al.*, 2015, 2016; Fernandez-Turiel *et al.*, 2013, 2014, 2015): the pre–caldera CB_1 unit, the syn–caldera CB_2 unit, and the post–caldera CB_3 unit (Table 1).

Deposits of the lowest unit CB_1 were interpreted as produced by block–and–ash flows from pre–caldera dome structures (Báez *et al.*, 2015, 2016). The mantled topography, the poorly defined stratification or parallel thin-bedding as well as the particle size (lapilli and mostly ash) of $CB_2$1 and $CB_2$2 deposits are consistent with air-fallout deposits from the buoyant eruption plume of a highly explosive eruption (Bagheri *et al.*, 2016; Cas & Wright, 1988). The lack of unconformities between $CB_2$1 and $CB_2$2 indicates no time gap between the emplacements of the deposits. The angular to sub–angular morphology of the pumice clasts and glass shards indicates a low degree of abrasion during transportation in the eruptive plume. The grain–size bimodality observed in primary distal $CB_2$1 and $CB_2$2 deposits (>100 km from source) is interpreted as evidence of particle aggregation and sedimentation of cored ash clusters. They are mostly sub–spherical fragile aggregates, observed with high–speed, high–resolution videos, that have never been observed in the deposits as they typically break at impact with the ground. They consist of a core particle (200–500 μm) fully covered by a thick shell of particles < 90 μm (Bagheri *et al.*, 2016; Brown *et al.*, 2012). The breaking of cored ash clusters and sedimentation of the integrating particles explain the bimodality in the distal $CB_2$1 and $CB_2$2 deposits, where the core particles are 100–400 μm in diameter and the shell particles are ~20 μm in diameter (Fig. 5c).

The $CB_2$3 sub–unit is interpreted as an ignimbrite massive lapilli–ash (mLT) lithofacies with inner transitions to diffuse–stratified lapilli–ash (dsLT) lithofacies, and changes to parallel and cross bedded lapilli–ash (//sLT and xsLT) lithofacies towards the top and on topographic highs (Branney & Kokelaar, 2002) as well as in distal regions. Lateral and vertical variations are related to changes in the pyroclastic

flow dynamics and their interactions with topography. The poorly defined stratification indicates pyroclastic flows under high depositional rates, transporting high concentrations of pumice and ash (Branney & Kokelaar, 2002; Cas *et al.*, 2011). The pumice imbrication shows the shear sense within the flow at that location. The interaction of these flows with the valley bottoms produced the ingestion of metamorphic and volcanic clasts from alluvial beds and terraces and incorporation into the bottom of ignimbrite. The change from a poorly defined stratification to parallel and cross–bedded structures evidences the action of traction–dominated flows, especially onto palaeohills. The last deposits were interpreted as stratified topographic veneers (Báez, 2014; Báez *et al.*, 2015).

Although there are no geochronological dates, the stratigraphy indicates that the paroxysmal phase of the eruption (CB_2 unit deposits) was followed by the emplacement of various lava domes ($CB_3$1 sub-unit) with associated fallout and phreatomagmatic deposits ($CB_3$2 sub-unit) (Báez *et al.*, 2016). The dispersion direction of the lobes, the structure of deposits, the absence of pumice and exotic lithic clasts, and the same rhyolitic composition shared by all components, all indicate an origin of $CB_3$3 sub-unit related to successive block–and–ash flows generated by gravitational or explosive lava–dome collapses (Charbonnier & Gertisser, 2008).

Finally, the siliceous sinters in the middle of the caldera ($CB_3$4) are interpreted as result of amorphous silica deposited around hot springs.

The Bolsón de Fiambalá sequence

The BdF_1 unit is interpreted as fallout deposits from the buoyant eruption plume of a highly explosive eruption (Cas & Wright, 1988). The overlying lapilli and ash deposits with heterogeneous clasts of regional rocks indicate reworking by water or wind (Figs. 3e and 4). Aeolian pumice–rich dunes are very common in the central and western areas of Bolsón de Fiambalá. Between BdF_1 unit and these overlying sediments there is evidence of a time gap, recorded by an erosional contact and occasional alluvial deposits.

The Nevado Tres Cruces Volcanic Complex, 90 km W of the Bolsón de Fiambalá basin, is the strongest candidate for the source of the BdF_1 deposits. Although proximal samples are not available to test this hypothesis, the geographical distribution, the geomorphological features observed in satellite images, and the petrological information from previous works (Baker *et al.*, 1987; Gardeweg *et al.*, 2000) describing the main trends of the stratigraphy and mineralogy (abundance of hornblende and biotite, and absence of K-feldspars) in the younger proximal dacitic ash-fall deposits, ignimbrites, and lava–domes of the Nevado Tres Cruces complex, favours this edifice as the possible source.

Implications of tephrochronology

Our results on tephra deposits of Southern Puna and neighbouring areas in NW Argentina are all consistent with three large eruptive events during the Holocene in the southern Puna and adjacent regions. Compositional data of glass and minerals (Figs. 10-14) and the unique occurrence of abundant large biotite crystals visible to the naked eye assist the association of the fallout deposits of Tolombón and Cafayate (CdP_1 unit) with the published Cerro Paranilla Ash of the Calchaquíes Valleys (Hermanns et al., 2000), whose age was established close to 7820 ±830 a BP. This age was obtained by ^{10}Be dating of a breakaway scarp of a rock–avalanche landslide directly overlying the ash (Hermanns & Schellenberger, 2008).

We found the fallout ash deposits of Cerro Blanco Volcanic Complex ($CB_2$1 and $CB_2$2) overlying a peat with an age of 4880 to 4780 a cal BP in Tafí del Valle). This age is consistent with the age of 4510 to 4240 a cal BP of a charred coal in a palaeosol underlying the ignimbrite ($CB_2$3) in Las Papas, and with the age of 4410 to 4100 a cal BP of charred material within this ignimbrite in Laguna Aguada Alumbrera (Figs. 7h, 9a, 9c). The fallout ash deposits of CBVC are correlated by stratigraphic relationship, chemical composition, mineralogy, and geochronology with previously described ash layers in the region: the mid–Holocene ash (Frenguelli, 1936), Ash C (Malamud *et al.*, 1996), volcanic ash layer (Wayne, 1999), Buey Muerto Ash (Hermanns & Schellenberger, 2008), and V1 ash layer (Sampietro-Vattuone & Peña-Monné, 2016) in the Calchaquíes Valleys and Tafí del Valle area, and with the volcanic

ash layer found in the archaeological site of Cueva Salamanca I near Antofagasta de la Sierra (Pintar, 2014). Furthermore, the $CB_2$3 ignimbrite dating is coherent with an age of an ignimbrite associated with CBVC (Montero-López *et al.*, 2010a). Combining the published ages with our results, the age of the eruptive event is likely closer to 4.2 ka cal BP.

The most recent fallout ash deposits of BdF_1 were identified as the V2 ash layer in the Calchaquíes Valleys and Tafí del Valle area (Sampietro Vattuone *et al.*, 2018; Sampietro-Vattuone & Peña-Monné, 2016). One fragment of a ceramic pot underlying the ash layer was TL (thermoluminiscence) dated 1772 ±112 a cal BP in Tafí del Valle (Sampietro-Vattuone & Peña-Monné, 2016). This age is coherent with those obtained from a charcoal (1520–1320 a cal BP) and a burnt basket (1400–1270 a cal BP), which were found beneath a reworked, 40 cm thick, pumiceous deposit of BdF_1 in the archaeological site of Palo Blanco (27°20'15.6"S, 67°44'36.4"W) (Fig. 3f) (Ratto, 2013). This deposit was identified by the amphibole phenocrysts. Finally, this ash layer was temporally located ca. 1500 AD in the Calchaquíes Valleys (Sampietro Vattuone *et al.*, 2018), but dating was done in a soil profile different to the profile where the V2 ash was observed. On the other hand, the oldest chronicle known in the area, related to the expedition of Diego de Almagro to Chile in 1536, does not relate any eruption during expedition or in previous years in the region (Ramón Folch, 1954). In our opinion, more work is needed to precise the age of this eruption.

Eruptive style of studied sequences

The three eruptions studied in this work were highly explosive and generated voluminous ash-fall deposits, non–welded ignimbrites, and lava dome extrusions. The extensive area of the voluminous fallout deposits of the CdP, CB and BdF sequences points towards a Plinian eruption style related to a great column height. We are in a preliminary phase of the study of the CdP and BdF sequences, which does not allow going further into describing the involved eruptions. Instead, the results from the CB sequence have enabled the identification of the most relevant features of the 4.2 ka cal BP Cerro Blanco eruption. Our findings corroborate previous results on the last eruptive event of the CBVC (Báez *et al.*, 2015; Fernandez-Turiel *et al.*, 2013, 2014, 2015), distinguishing pre–, syn–, and post–caldera products, and allow us to estimate the large extent of the Plinian fallout during the paroxysmal phase of the eruption.

The pre–caldera phase of the Cerro Blanco eruption

The post-depositional dissection of the block–and–ash flow deposits of CB_1 by the caldera edge allows the interpretation that it is a pre–caldera unit from an extrusive dome that is compositionally linked to CB. Therefore, this unit is included in the CB sequence assisted by its similar petrography and geochemistry to the other CB units that differentiate them from the older products of the CBVC (Báez *et al.*, 2015; Montero-López *et al.*, 2010b).

The syn–caldera phase of the Cerro Blanco eruption

The lack of geochronological data does not allow estimation of the time gap between CB_1 and CB_2, i.e., the caldera collapse. The absence of lithic breccias or pyroclastic products around the caldera edges, as well as the low lithic content in pyroclastic products of CB_2, suggest that a single vent in the SW of the caldera rim acted as emission conduit during the eruption, favouring optimal conditions for a sustained Plinian column and fallout deposition.

The fall deposit $CB_2$1 of alternating layers, 1-3 cm thick, some of lapilli and some of ash are the first record of the Plinian column. The lower thickness of this deposit among CB_2 sub–units seems to be consistent with a relatively brief episode in comparison with those generating the overlying sub–units. Thin bedding suggests instability because of changing column heights and therefore variable vertical wind patterns (Cioni *et al.*, 2000). The change to the thicker, unstratified rhyolitic ash ($CB_2$2) indicates that the feeding system reached and maintained steady conditions during a single climactic column phase (Cioni *et al.*, 2000; Pardo *et al.*, 2012). The eruption column height for this phase reached 27 km, according the results of Tephra2 modelling, with an ESE dispersal on a large surface of the Chacopampean Plain (Fernandez-Turiel *et al*., 2019; Fig. S3).

Bimodal particle size distributions, as observed in $CB_2$1 and $CB_2$2, are a common feature in many distal ash deposits, such as in the eruptions of Campanian Ignimbrite (CI) 39 ka BP (Engwell *et al.*, 2014), Pinatubo in 1991 (Wiesner *et al.*, 2004), and Chaitén in 2008 (Durant *et al.*, 2012; Ruggieri *et al.*, 2012; Watt *et al.*, 2009). The occurrence of these particle size subpopulations in fallout deposits was explained by the propensity of aggregation in historic and ancient eruptions, independently of their style (Brown *et al.*, 2012; Durant *et al.*, 2009, 2012), but also by other processes without the need for aggregation, e.g., particle differences in texture and componentry, convective instabilities in eruptive plume, and lower atmospheric circulation patterns (Durant *et al.*, 2009; Watt *et al.*, 2015).

An interesting new approach to explain the particle size bimodality is through particulate cored clusters. They are sub–spherical fragile aggregates consisting of a core particle of hundreds of microns in size covered by a thick shell of particles of tens of microns in diameter (Bagheri *et al.*, 2016). These aggregates are formed in the buoyant column and plume of the eruption. These ash clusters tend to disaggregate on impact with the ground and, as consequence of their very low preservation potential, they are difficult to find and document in the historic and ancient ash-fall deposits, although their presence can be inferred by polymodal particle size populations. In this way, the bimodality of the Plinian $CB_2$1 and $CB_2$2 sub–units from 100 km away from the Cerro Blanco through more than 350 km (Fig. 5c) could be due to the clustering phenomena of the ashes described in the literature.

A distal mass accumulation maximum or secondary thickening was observed in many historic ash-fall deposits. For example, in the eruptions of Quizapú, Chile in 1932 (Hildreth & Drake, 1992), Mt. St. Helens, Washington, USA in 1980 (Carey & Sigurdsson, 1982; Sarna-Wojcicki *et al.*, 1982), Unzen, Japan in 1991 (Watanabe *et al.*, 1999), Mt. Hudson, Chile in 1991 (Scasso *et al.*, 1994), Pinatubo, Philippines in 1991 (Wiesner *et al.*, 2004), Crater Peak, Alaska, USA in 1992 (McGimsey *et al.*, 2001), and Chaitén, Chile in 2008 (Watt *et al.*, 2009). This phenomenon has been related to ash aggregation in the eruptive plume (Brown *et al.*, 2012; Carey & Sigurdsson, 1982). Aggregation may be enhanced by the freezing of water in the high troposphere and the melting of the ice in aggregates is postulated as the mechanism that triggers their fall *en masse* (Brown *et al.*, 2012; Mastin *et al.*, 2016).

The distal mass accumulation maximum of the Plinian $CB_2$2 sub–unit reached several meters thick ~210 km from the volcano, in the eastern ranges that surrounds the southern Puna (Figs. 6, 7e, 7f, and Fernandez-Turiel *et al*., 2019; Fig. S4). Semi–arid conditions prevail west of this area, while warm, moist, and rainy conditions prevail over the easternmost slopes of these ranges and adjacent lowlands. The climate of Central Andes is characterized by a complex interplay of large–scale atmospheric circulation with local orographic effects (Garreaud *et al.*, 2003; Garreaud, 2009; Neukom *et al.*, 2015), and the main moisture source for the region is the easterly influx from the Amazon Basin. In this setting, the eastern upslope moist warm flow could accentuate the ice melting in aggregates, collapsing their structure and triggering ash-fall *en masse*.

The secondary thickening related to upslope moisture transport by easterly atmospheric flow, should also elucidate the presumable secondary thickenings of the Cueros de Purulla eruption near Cafayate, where there are several metre-thick fallout ash deposits of CdP_1 (Fig. 3b), and the BdF_1 ashes in the northwest of Bolsón de Fiambalá (Fernandez-Turiel *et al*., 2019; Fig. S4). However, the warm and moist easterlies hardly reach these areas implying that these deposits have not necessarily affected by wet disaggregation and that other process may be highly significant in driving the fallout of particles. If we observe the location of the secondary thickenings for CdP, CB and BdF fallout units in topographic profiles (Fernandez-Turiel *et al*., 2019; Fig. S4), the affected areas are in the eastern slopes of important ranges. This fact allows us to consider in the conceptual model the effect of the topographically induced turbulences in the disaggregation, e.g., the breaking of lee waves, generated by winds passing over elevated topography beneath the eruption plume (Watt *et al.*, 2015). As a consequence, this spatial association of the secondary thickening and topography could help to locate affected areas in similar cases. It may also help to prevent hazards associated with the increased loading of ash on infrastructures and buildings (Wilson *et al.*, 2014), because it allows us

to constrain more precisely the most hazardous areas during large explosive eruptions around the world and, particularly, in the Central Volcanic Zone of Andes, which are the eastern slopes of the mountain ranges bordering the Altiplano–Puna plateau.

The $CB_2$3 PDC's maybe were partially synchronous with the $CB_2$2 ash-fall. Many Plinian columns generate regional fall deposits and large-volume ignimbrites at the same time. Marginal collapse forms PDC's while central column sends up regional fall (e.g., Bishop Tuff, 1912 Novarupta) (Hildreth & Fierstein, 2012a). The transition to non–optimal conditions for a buoyant column, possibly with a significant increase in discharge rates, may also produce large PDCs preceding caldera collapse (Legros, 2000).

Thus, on the whole, the CB_2 unit follows the idealised sequence of a caldera–forming eruption, displaying a Plinian fall deposit overlain by an ignimbrite (Druitt & Sparks, 1984; Legros *et al.*, 2000). However, in the Cerro Blanco caldera this model is more complex, as is revealed by the two different compositions of plagioclases, biotite, and Fe–Ti oxides observed in the CB_2 syn–caldera sub–units which seem to indicate mixing of two magma batches during the eruption. The compositional homogeneity of CB_1 and CB_3 deposits suggests a single magma body. Within the paroxysm of the eruption, however, it is likely that another significant magma input occurred, recorded in the compositional bimodality of CB_2 deposits. The most frequent compositions in CB_2 are also the same as the most common observed in CB_1 and CB_3 (Figs. 10–14). A possible explanation for the minority compositions could be the mobilization of hotter magma, evidenced by geothermobarometry data, from a different part of the magmatic chamber. Similar mixing–derived bimodality was observed in titanomagnetite compositions of magmatic products from, for example, Mono Basin in California (Marcaida *et al.*, 2014) and Usu volcano in Japan (Tomiya & Takahashi, 2005).

The post–caldera phase of the Cerro Blanco eruption

There are no geochronological data to determine the time gap between the syn–caldera CB_2 and the post–caldera CB_3 units. The CB_3 unit represents a significant change in the eruption style of the CBVC, from an explosive phase (CB_2) to an essentially effusive magmatic phase characterised by the extrusion of the $CB_3$1 lava domes in the SW edge of the Cerro Blanco caldera, and the occurrence of different fallout episodes of pyroclasts and block–and–ash flows related to them. Block–and–ash flows were topographically confined towards the caldera's interior, filling the bottom of this 5 km wide circular structure almost completely (Fig. 2a). These flows involved both single and multiple–collapse events such as those documented in the eruptions of Unzen in Japan, Colima in Mexico, Merapi in Indonesia, Arenal in Costa Rica, and Montserrat in Lesser Antilles (Charbonnier & Gertisser, 2008; Freundt *et al.*, 2000). A post–eruption geothermal field produced white sinter deposits within the Cerro Blanco caldera. The associated hot springs, located in the central part of the caldera, are active in the present day (Viramonte *et al.*, 2005). Finally, the Cerro Blanco caldera area showed a deformation pattern subsiding about 1-3 cm/year at least since 1992 (Pritchard & Simons, 2004, Brunori *et al.*, 2013, Henderson & Pritchard, 2013, Yazdanparast *et al.*, 2017).

Volcanic explosivity index of 4.2 cal BP CBVC eruption

Only proximal and medial fallout deposit thickness data, reaching 400 km eastward, are available for the Cerro Blanco eruption, which is common in many prehistoric deposits (Bonadonna & Houghton, 2005). Consequently, large uncertainties in volume estimates are expected. Despite this, the order of magnitude obtained for bulk volume estimates always exceeds 100 km^3, i.e., the threshold value for a volcanic explosivity index or VEI of 7 (Fernandez-Turiel *et al.*, 2013, 2014, 2015). Taking as a point of reference the density of the 2008 Chaitén rhyolitic ash deposits, that ranged from 1,000 to 1,250 $kg \cdot m^{-3}$ (Alfano *et al.*, 2011; Watt *et al.*, 2009), we have assumed a deposit density of 1,000 $kg \cdot m^{-3}$ excluding lithics. With this value and a dense–rock density of 2,300 $kg \cdot m^{-3}$, the 172 km^3 of bulk volume amounts to a dense–rock equivalent (DRE) volume of 75 km^3. Based on a model of the pre–eruptive topography, the volume of ignimbrite associated with Cerro Blanco accumulated 15 km^3 without lithics (Báez et al., 2015), corresponding to 8.5 km^3 DRE,

assuming a bulk density of 1,300 kg·m^{-3}, and a dense–rock density of 2,300 kg·m^{-3}. Based on these results, the Cerro Blanco eruption is among the largest volcanic eruptions of the Holocene globally, similar to Kuril Lake (Kamchatka, Russia), Crater Lake (Oregon, USA), Tambora (Indonesia), Samalas (Indonesia), Aniakchak (Alaska, USA), Santorini (Greece), or Changbaishan (China–North Corea) (Brown *et al.*, 2014; Crosweller *et al.*, 2012; Lavigne *et al.*, 2013; Vidal *et al.*, 2015). It clearly exceeds the magnitude of the 1600 Huaynaputina eruption, the largest historical eruption known in the Central Volcanic Zone of the Andes (Global Volcanism Program, 2013b; Stern, 2004; Tilling, 2009).

Conclusions

Results confirm the existence of three major rhyolitic eruptive events during Holocene in the southern Puna and neighbouring areas, and provide a more complete picture of the style, frequency, distribution, and size of past explosive eruptions in the region. The Cerro Blanco Volcanic Complex (the focus of this work) is demonstrated as source of the 4.2 ka cal BP pyroclastic deposits, whereas Cueros de Purulla volcano is suggested as the origin of the Lower Holocene pyroclastic deposits, and the Nevado Tres Cruces Volcanic Complex is the strongest candidate for the source of the Upper Holocene pyroclastic deposits found in the Bolsón de Fiambalá basin.

Based on 1) field observations (stratigraphic and geomorphological relationships, structure, and thickness of deposits), 2) petrography and geochemistry of juvenile eruptive products, 3) ^{14}C ages, and 4) erupted volume, we conclude that the CBVC generated the largest documented eruption during the past five millennia in the Central Volcanic Zone of Andes and one of the largest around the world for this period. Cerro Blanco ash-fall deposits reached >400 km from the vent indicating that ~170 km^3 of ash were spread around 500,000 km^2 in Argentina, while pyroclastic flow deposits extended north, northwest, and south several tens of kilometres from the vent.

The implications of the findings of the present work reach far beyond having some chronostratigraphic markers. Further interdisciplinary research should be performed in order to draw general conclusions on these impacts in local environments and the disruptive consequences for local communities. This is invaluable not just for understanding how the system may have been affected over time, but also for evaluating volcanic hazards and risk mitigation measures related to potential future large explosive eruptions.

ACKNOWLEDGMENTS

Financial support was provided by the ASH and QUECA Projects (MINECO, CGL2008–00099 and CGL2011–23307). We acknowledge the assistance in the analytical work of labGEOTOP Geochemistry Laboratory (infrastructure co–funded by ERDF–EU Ref. CSIC08–4E–001) and DRX Laboratory (infrastructure co–funded by ERDF–EU Ref. CSIC10–4E–141) (J. Ibañez, J. Elvira and S. Alvarez) of ICTJA-CSIC, and EPMA and SEM Laboratories of CCiTUB (X. Llovet and J. Garcia Veigas). This study was carried out in the framework of the Research Consolidated Groups GEOVOL (Canary Islands Government, ULPGC) and GEOPAM (Generalitat de Catalunya, 2017 SGR 1494). We thank F. Ruggieri, G. Galindo, L. D. Martínez, R. A. Gil, A. Storniolo and D. Rodriguez for their collaboration in different aspects of this work; A. Tindle and G. Droop for the Structural Formula Calculators for microprobe data; and W. Vaughan for the spreadsheets for ternary plots. We thank W. Báez, R. I. Tilling, J. Fierstein, S. Kutterolf and the anonymous reviewers for their comments and ideas that helped to significantly improve an earlier version of the manuscript. We thank A. Wall for his support in editing the English.

References

Alfano, F.; Bonadonna, C.; Volentik, A.C.M.; Connor, C.B.; Watt, S.F.L.; Pyle, D.M. & Connor, L.J. (2011). Tephra stratigraphy and eruptive volume of the May, 2008, Chaitén eruption, Chile. Bulletin of Volcanology, 73: 613–630. https://doi.org/10.1007/s00445-010-0428-x

Arnosio, M.; Becchio, R.; Viramonte, J.; Groppelli, G.; Norini, G. & Corazzato, C. (2005). Geología del Complejo Volcánico Cerro Blanco (26o 45' S-67o 45'O), Puna Austral. XVI Congreso Geológico Argentino.

Arnosio, M.; Becchio, R.; Viramonte, J.G.; De Silva, S. & Viramonte, J.M. (2008). Geocronología e isotopía del Complejo Volcánico Cerro Blanco: un sistema de calderas cuaternario (73 - 12 ka) en los Andes centrales del sur. XVII Congreso Geológico Argentino.

Aulinas, M.; Garcia-Valles, M.; Fernandez-Turiel, J.L.; Gimeno, D.; Saavedra, J. & Gisbert, G. (2015). Insights into the formation of rock varnish in prevailing dusty regions. Earth Surface Processes and Landforms, 40: 447–458. https://doi.org/10.1002/esp.3644

Báez, W. (2014). Estratigrafía volcánica, estilos eruptivos y evolución del Complejo Volcanico Cerro Blanco, Puna Austral. Ph. D., Salta, Argentina, Universidad Nacional de Salta, 204 pp.

Báez, W.; Arnosio, M.; Chiodi, A.; Ortíz-Yañes, A.; Viramonte, J.G.; Bustos, E.; Giordano, G. & López, J.F. (2015). Estratigrafía y evolución del Complejo Volcánico Cerro Blanco, Puna Austral, Argentina. Revista Mexicana De Ciencias Geologicas, 32: 29–49.

Báez, W.A.; Chiodi, A.; Bustos, E.; Arnosio, M.; Viramonte, J.G.; Giordano, G. & Alfaro Ortega, B. (2016). Mecanismos de emplazamiento y destrucción de los domos lávicos asociados a la caldera del Cerro Blanco, Puna Austral. Revista de la Asociación Geológica Argentina; Vol 74, No 2 (2017).

Bagheri, G.; Rossi, E.; Biass, S. & Bonadonna, C. (2016). Timing and nature of volcanic particle clusters based on field and numerical investigations. Journal of Volcanology and Geothermal Research, 327: 520–530. https://doi.org/10.1016/j.jvolgeores.2016.09.009

Baker, P.E.; Gonzalez-Ferran, O. & Rex, D.C. (1987). Geology and geochemistry of the Ojos del Salado volcanic Region, Chile. Journal of the Geological Society, 144: 85–96. https://doi.org/10.1144/gsjgs.144.1.0085

Bianchi, M. et al. (2013). Teleseismic tomography of the southern Puna plateau in Argentina and adjacent regions. Tectonophysics, 586: 65–83. https://doi.org/10.1016/j.tecto.2012.11.016

Bonadonna, C.; Connor, C.B.; Houghton, B.F.; Connor, L.; Byrne, M.; Laing, A. & Hincks, T.K. (2005). Probabilistic modeling of tephra dispersal: Hazard assessment of a multiphase rhyolitic eruption at Tarawera, New Zealand. Journal of Geophysical Research: Solid Earth, 110. https://doi.org/10.1029/2003JB002896

Bonadonna, C. & Houghton, B.F. (2005). Total grain-size distribution and volume of tephra-fall deposits. Bulletin of Volcanology, 67: 441–456. https://doi.org/10.1007/s00445-004-0386-2

Branney, M.J. & Kokelaar, P. (2002). Pyroclastic density currents and the sedimentation of ignimbrites. Geological Society, London, 143 pp.

Brazier, S.; Sparks, R.S.J.; Carey, S.N.; Sigurdsson, H. & Westgate, J.A. (1983). Bimodal grain size distribution and secondary thickening in air-fall ash layers. Nature, 301: 115–119. https://doi.org/10.1038/301115a0

Bronk Ramsey, C. (2009). Bayesian analysis of radiocarbon dates. Radiocarbon, 51: 337–360. https://doi.org/10.1017/S0033822200033865

Brown, R.J.; Bonadonna, C. & Durant, A.J. (2012). A review of volcanic ash aggregation. Physics and Chemistry of the Earth, Parts A/B/C, 45–46: 65–78. https://doi.org/10.1016/j.pce.2011.11.001

Brown, S. et al. (2014). Characterisation of the Quaternary eruption record: analysis of the Large Magnitude Explosive Volcanic Eruptions (LaMEVE) database. Journal of Applied Volcanology, 3: 5. https://doi.org/10.1186/2191-5040-3-5

Brunori, C.A.; Bignami, C.; Stramondo, S. & Bustos, E. (2013). 20 years of active deformation on volcano caldera: Joint analysis of InSAR and AInSAR techniques. International Journal of Applied Earth Observation and Geoinformation, 23: 279–287. https://doi.org/10.1016/j.jag.2012.10.003

Carey, S.N. & Sigurdsson, H. (1982). Influence of particle aggregation on deposition of distal tephra from the May 18, 1980, eruption of Mount St. Helens volcano. Journal of Geophysical Research: Solid Earth, 87: 7061–7072. https://doi.org/10.1029/JB087iB08p07061

Cas, R.; Porritt, L.; Pittari, A. & Hayman, P. (2008). A new approach to kimberlite facies terminology using a revised general approach to the nomenclature of all volcanic rocks and deposits: Descriptive to genetic. Journal of Volcanology and Geothermal Research, 174: 226–240. https://doi.org/10.1016/j.jvolgeores.2007.12.018

Cas, R. & Wright, J. (1988). Volcanic Successions Modern and Ancient. A geological approach to processes, products and successions. Springer Netherlands, 528 pp.

Cas, R.A.F.; Wright, H.M.N.; Folkes, C.B.; Lesti, C.; Porreca, M.; Giordano, G. & Viramonte, J.G. (2011). The flow dynamics of an extremely large volume pyroclastic flow, the 2.08-Ma Cerro Galán Ignimbrite, NW Argentina, and comparison with other flow types. Bulletin of Volcanology, 73: 1583–1609. https://doi.org/10.1007/s00445-011-0564-y

Charbonnier, S.J. & Gertisser, R. (2008). Field observations and surface characteristics of pristine block-and-ash flow deposits from the 2006 eruption of Merapi Volcano, Java, Indonesia. Journal of Volcanology and Geothermal Research, 177: 971–982. https://doi.org/10.1016/j.jvolgeores.2008.07.008

Cioni, R.; Marianelli, P.; Santacroce, R. & Sbrana, A. (2000). Plinian and subplinian eruptions. In: Encyclopaedia of Volcanoes (Sigurdsson, H.; Houghton, B. F.; McNutt, S. R.; Rymer, H. & Stix, J., eds.). Academic Press, San Diego, 477–494.

Connor, L.J. & Connor, C.B. (2006). Inversion is the key to dispersion: understanding eruption dynamics by inverting tephra fallout. (Mader, H. M.; Coles, S. G.; Connor, C. B. & Connor, L. J., eds.). In: Statistics in Volcanology. Geological Society of London.

Crosweller, H.S. et al. (2012). Global database on large magnitude explosive volcanic eruptions (LaMEVE). Journal of Applied Volcanology, 1: 4. https://doi.org/10.1186/2191-5040-1-4

Daggitt, M.L.; Mather, T.A.; Pyle, D.M. & Page, S. (2014). AshCalc–a new tool for the comparison of the exponential, power-law and Weibull models of

tephra deposition. Journal of Applied Volcanology, 3: 7. https://doi.org/10.1186/2191-5040-3-7

Druitt, T.H. & Sparks, R.S.J. (1984). On the formation of calderas during ignimbrite eruptions. Nature, 310: 679–681. https://doi.org/10.1038/310679a0

Durant, A.J.; Rose, W.I.; Sarna-Wojcicki, A.M.; Carey, S. & Volentik, A.C.M. (2009). Hydrometeor-enhanced tephra sedimentation: Constraints from the 18 May 1980 eruption of Mount St. Helens. Journal of Geophysical Research: Solid Earth, 114: B03204. https://doi.org/10.1029/2008JB005756

Durant, A.J.; Villarosa, G.; Rose, W.I.; Delmelle, P.; Prata, A.J. & Viramonte, J.G. (2012). Long-range volcanic ash transport and fallout during the 2008 eruption of Chaitén volcano, Chile. Physics and Chemistry of the Earth, 45–46: 50–64. https://doi.org/10.1016/j.pce.2011.09.004

Engwell, S.L.; Sparks, R.S.J. & Carey, S. (2014). Physical characteristics of tephra layers in the deep sea realm: The Campanian Ignimbrite eruption. Geological Society, London, Special Publications, 398. https://doi.org/10.1144/SP398.7

Erdmann, S.; Martel, C.; Pichavant, M. & Kushnir, A. (2014). Amphibole as an archivist of magmatic crystallization conditions: problems, potential, and implications for inferring magma storage prior to the paroxysmal 2010 eruption of Mount Merapi, Indonesia. Contributions to Mineralogy and Petrology, 167: 1016. https://doi.org/10.1007/s00410-014-1016-4

Fernandez-Turiel, J.L. et al. (2015). The ash deposits of the 4200 BP Cerro Blanco eruption: the largest Holocene eruption of the Central Andes. EGU General Assembly, EGU2015-3392.

Fernandez-Turiel, J.L.; Perez-Torrado, F.J.; Saavedra, J.; Osterrieth, M. & Carrizo, J.I. (2014). Cerro Blanco originó la mayor erupción de los últimos 5000 años en el noroeste de Argentina. Actas, XIX Congreso Geológico Argentino, 1093–1094.

Fernandez-Turiel, J.L.; Perez-Torrado, F. J.; Rodriguez-Gonzalez, A.; Saavedra, J.; Carracedo, J. C., Rejas, M.; Lobo, A.; Osterrieth, M.; Carrizo, J. I.; Esteban, G.; Gallardo, J. & Ratto, N. (2019). Dataset of SEM images, modelled isopach map and topographic profiles, radiocarbon ages and data of parameters of Tephra2 and AshCalc codes of Holocene volcanic ashes of NW Argentina. In: DIGITAL.CSIC, http://hdl.handle.net/10261/179003.

Fernandez-Turiel, J.L.; Rejas, M.; Perez-Torrado, F.J.; Saavedra, J. & Rodriguez-Gonzalez, A. (2018a). Dataset of geochemical data of Holocene volcanic ashes of NW Argentina. DIGITAL.CSIC, http://hdl.handle.net/10261/167757.

Fernandez-Turiel, J.L.; Rejas, M.; Perez-Torrado, F.J.; Saavedra, J. & Rodriguez-Gonzalez, A. (2018b). Dataset of particle size distribution data of Holocene volcanic ashes of NW Argentina. DIGITAL.CSIC, http://hdl.handle.net/10261/167764.

Fernandez-Turiel, J.L.; Saavedra, J.; Perez-Torrado, F.J.; Rodriguez-Gonzalez, A.; Carracedo, J.C.; Osterrieth, M.; Carrizo, J.I. & Esteban, G. (2013). The largest Holocene eruption of the Central Andes found. AGU Fall Meeting.

Fierstein, J. & Hildreth, W. (1992). The plinian eruptions of 1912 at Novarupta, Katmai National Park, Alaska. Bull Volcanol, 54: 646–684. https://doi.org/10.1007/BF00430778

Fierstein, J. & Nathenson, M. (1992). Another look at the calculation of fallout tephra volumes. Bull Volcanol, 54: 156–167. https://doi.org/10.1007/BF00278005

Fontijn, K.; Lachowycz, S.M.; Rawson, H.; Pyle, D.M.; Mather, T.A.; Naranjo, J.A. & Moreno-Roa, H. (2014). Late Quaternary tephrostratigraphy of southern Chile and Argentina. Quaternary Science Reviews, 89: 70–84. https://doi.org/10.1016/j.quascirev.2014.02.007

Frenguelli, J. (1936). Investigaciones geológicas en la zona salteña del valle de Santa María. Obra del Cincuentenario del Museo de La Plata. In: Obra del Cincuentenario del Museo de La Plata. La Plata, 215–572.

Freundt, A.; Wilson, C.J.N. & Carey, S.N. (2000). Ignimbrites and block-and-ash flow deposits. (Sigurdsson, H.; Houghton, B. F.; McNutt, S. R.; Rymer, H. & Stix, J., eds.). In: Encyclopaedia of Volcanoes. Academic Press, San Diego, 581–599.

Gardeweg, M.; Clavero, J.; Mpodozis, C.; Pérez de A., C. & Villeneuve, M. (2000). El Macizo Tres Cruces: un complejo volcánico longevo y potencialmente activo en la Alta Cordillera de Copiapó, Chile. Actas IX Congreso Geológico Chileno, Simposio Geología y Recursos Minerales de los Andes Centrales, avances del Proyecto Multinacional Andino, MAP, 291–295.

Garreaud, R.; Vuille, M. & Clement, A.C. (2003). The climate of the Altiplano: observed current conditions and mechanisms of past changes. Palaeogeography, Palaeoclimatology, Palaeoecology, 194: 5–22. https://doi.org/10.1016/S0031-0182(03)00269-4

Garreaud, R.D. (2009). The Andes climate and weather. Adv. Geosci., 22: 3–11. https://doi.org/10.5194/adgeo-22-3-2009

Ghiorso, M.S. & Evans, B.W. (2008). Thermodynamics of Rhombohedral Oxide Solid Solutions and a Revision of the FE-TI Two-Oxide Geothermometer and Oxygen-Barometer. American Journal of Science, 308: 957–1039. https://doi.org/10.2475/09.2008.01

Gilbert, D.; Freundt, A.; Kutterolf, S. & Burkert, C. (2014). Post-glacial time series of explosive eruptions and associated changes in the magma plumbing system of Lonquimay volcano, south central Chile. International Journal of Earth Sciences, 103: 2043–2062. https://doi.org/10.1007/s00531-012-0796-x

Global Volcanism Program, 2013a. Volcanoes of the World, v. 4.7.4. Venzke, E (ed.). Smithsonian

Institution. Downloaded 01 Dec 2018 (https://volcano.si.edu/volcano.cfm?vn=355210). https://doi.org/10.5479/si.GVP.VOTW4-2013.

Global Volcanism Program, 2013b. Cerro Blanco (355210) in Volcanoes of the World, v. 4.7.4. Venzke, E (ed.). Smithsonian Institution. Downloaded 01 Dec 2018 (https://volcano.si.edu/volcano.cfm?vn=355210). https://doi.org/10.5479/si.GVP.VOTW4-2013.

Global Volcanism Program, 2013c. Huaynaputina (354030) in Volcanoes of the World, v. 4.7.4. Venzke, E (ed.). Smithsonian Institution. Downloaded 01 Dec 2018 (https://volcano.si.edu/volcano.cfm?vn=354030#). https://doi.org/10.5479/si.GVP.VOTW4-2013.

Henderson, S.T. & Pritchard, M.E. (2013). Decadal volcanic deformation in the Central Andes Volcanic Zone revealed by InSAR time series. Geochemistry, Geophysics, Geosystems, 14: 1358–1374.

Hermanns, R.L. & Schellenberger, A. (2008). Quaternary tephrochronology helps define conditioning factors and triggering mechanisms of rock avalanches in NW Argentina. Quaternary International, 178: 261–275. https://doi.org/10.1016/j.quaint.2007.05.002

Hermanns, R.L.; Trauth, M.H.; Niedermann, S.; McWilliams, M. & Strecker, M.R. (2000). Tephrochronologic constraints on temporal distribution of large landslides in northwest Argentina. Journal of Geology, 108: 35–52. https://doi.org/10.1086/314383

Hildreth, W. & Drake, R.E. (1992). Volcan Quizapu, Chilean Andes. Bulletin of Volcanology, 54: 93–125. https://doi.org/10.1007/BF00278002

Hildreth, W. & Fierstein, J. (2012a). The Novarupta-Katmai eruption of 1912—largest eruption of the twentieth century; centennial perspectives. U.S. Geological Survey Professional Paper, 1791: 1–259.

Hildreth, W. & Fierstein, J. (2012b). Eruptive history of Mount Katmai, Alaska. Geosphere, 8: 1527–1567. https://doi.org/10.1130/GES00817.1

Hogg, A.G. et al. (2013). SHCal13 Southern Hemisphere Calibration, 0–50,000 Years cal BP. Radiocarbon, 55: 1889–1903. https://doi.org/10.2458/azu_js_rc.55.16783

Houghton, B. & Carey, R. J. (2015). Pyroclastic fall deposits. In: Encyclopedia of volcanoes. Academic Press, London, 599–616. https://doi.org/10.1016/B978-0-12-385938-9.00034-1

Jenkins, S. F.; Wilson, T. M.; Miller, V.; Stewart, C.; Marzocchi, W. & Boulton, M. (2015). Volcanic ash fall hazard and risk: Technical Background Paper for the UNISDR 2015 Global Assessment Report on Disaster Risk Reduction. Global Volcano Model and IAVCEI, 43.

Kay, S.M.; Coira, B. & Mpodozis, C. (2006). Late Neogene volcanism in the Cerro Blanco region of the Puna Austral, Argentina (26.5oS 67.5oW). XI Congreso Geológico Chileno, 499–502.

Kay, S.M.; Coira, B. & Mpodozis, C. (2008). Field trip guide: Neogene evolution of the central Andean Puna plateau and southern Central Volcanic Zone. Field Guides, 13: 117–181. https://doi.org/10.1130/2008.0013(05)

Kay, S.M.; Coira, B.L.; Caffe, P.J. & Chen, C.H. (2010). Regional chemical diversity, crustal and mantle sources and evolution of central Andean Puna plateau ignimbrites. Journal of Volcanology and Geothermal Research, 198: 81–111. https://doi.org/10.1016/j.jvolgeores.2010.08.013

Lane, C.S.; Lowe, D.J.; Blockley, S.P.E.; Suzuki, T. & Smith, V.C. (2017). Advancing tephrochronology as a global dating tool: Applications in volcanology, archaeology, and palaeoclimatic research. Quaternary Geochronology, 40: 1–7.

Lavigne, F. et al. (2013). Source of the great A.D. 1257 mystery eruption unveiled, Samalas volcano, Rinjani Volcanic Complex, Indonesia. Proceedings of the National Academy of Sciences, 110: 16742–16747. https://doi.org/10.1073/pnas.1307520110

Legros, F. (2000). Minimum volume of a tephra fallout deposit estimated from a single isopach. Journal of Volcanology and Geothermal Research, 96: 25–32. https://doi.org/10.1016/S0377-0273(99)00135-3

Legros, F.; Kelfoun, K. & Martí, J. (2000). The influence of conduit geometry on the dynamics of caldera-forming eruptions. Earth and Planetary Science Letters, 179: 53–61. https://doi.org/10.1016/S0012-821X(00)00109-6

Locock, A.J. (2014). An Excel spreadsheet to classify chemical analyses of amphiboles following the IMA 2012 recommendations. Computers & Geosciences, 62: 1–11. https://doi.org/10.1016/j.cageo.2013.09.011

Lowe, D.J. (2011). Tephrochronology and its application: A review. Quaternary Geochronology, 6: 107–153. https://doi.org/10.1016/j.quageo.2010.08.003

Malamud, B.D.; Jordan, T.E.; Alonso, R.A.; Gallardo, E.F.; González, R.E. & Kelley, S.A. (1996). Pleistocene Lake Lerma, Salta Province, NW Argentina. XIII Congreso Geológico Argentino y III Congreso de Exploración de Hidrocarburos, 103–114.

Marcaida, M.; Mangan, M.T.; Vazquez, J.A.; Bursik, M. & Lidzbarski, M.I. (2014). Geochemical fingerprinting of Wilson Creek formation tephra layers (Mono Basin, California) using titanomagnetite compositions. Journal of Volcanology and Geothermal Research, 273: 1–14. https://doi.org/10.1016/j.jvolgeores.2013.12.008

Mastin, L.G.; Van Eaton, A.R. & Durant, A.J. (2016). Adjusting particle-size distributions to account for aggregation in tephra-deposit model forecasts. Atmos. Chem. Phys., 16: 9399–9420. https://doi.org/10.5194/acp-16-9399-2016

McGimsey, R.G.; Neal, C.A. & Riley, C.M. (2001). Areal distribution, thickness, mass, volume, and grain size

of tephra-fall deposits from the 1992 eruptions of Crater Peak Vent, Mt. Spurr Volcano, Alaska. U. S. Geological Survey, 38 pp. https://doi.org/10.3133/ofr01370

Montero-López, M.C.; Hongn, F.; Brod, J.A.; Seggiaro, R.; Marrett, R. & Sudo, M. (2010a). Magmatismo ácido del Mioceno Superior-Cuaternario en el área de Cerro Blanco- La Hoyada, Puna Austral. Revista de la Asociación Geológica Argentina, 67: 329–348.

Montero-López, M.C.; Hongn, F.; Seggiaro, R.; Brod, J.A. & Marrett, R. (2010b). Estratigrafía y geoquímica del volcanismo de composición intermedia (Mioceno Superior-Plioceno) en el extremo oriental de la cordillera de San Buenaventura (Puna Austral). Revista de la Asociación Geológica Argentina, 67: 112–129.

Montero-López, M.C.; Hongn, R.; Seggiaro, R.; Marrett, R. & Ratto, N. (2009). Relación entre el volcanismo y los registros arqueológicos en el bolsón de Fiambalá (Departamento Tinogasta, Catamarca). In: Entrelazando Ciencias: Sociedad y ambiente antes de la conquista española (Ratto, N., ed.). EUDEBA, Buenos Aires, 131–158.

Neukom, R.; Rohrer, M.; Calanca, P.; Salzmann, N.; Huggel, C.; Acuña, D.; Christie, D. & Morales, M.S. (2015). Facing unprecedented drying of the Central Andes? Precipitation variability over the period AD 1000–2100. Environmental Research Letters, 10: 084017.

Pardo, N.; Cronin, S.J.; Palmer, A.S. & Németh, K. (2012). Reconstructing the largest explosive eruptions of Mt. Ruapehu, New Zealand: lithostratigraphic tools to understand subplinian–plinian eruptions at andesitic volcanoes. Bulletin of Volcanology, 74: 617–640. https://doi.org/10.1007/s00445-011-0555-z

Pignatelli, I.; Faure, F. & Mosser-Ruck, R. (2016). Self-mixing magma in the Ruiz Peak rhyodacite (New Mexico, USA): A mechanism explaining the formation of long period polytypes of mica. Lithos, 266–267: 332–347. https://doi.org/10.1016/j.lithos.2016.10.024

Pintar, E. (2014). Continuidades e hiatos ocupacionales durante el holoceno medio en el borde oriental de la Puna Salada, Antofagasta de la Sierra, Argentina. Chungará (Arica), 46: 51–72. https://doi.org/10.4067/S0717-73562014000100004

Ponomareva, V.; Portnyagin, M. & Davies, S.M. (2015). Tephra without Borders: Far-Reaching Clues into Past Explosive Eruptions. Frontiers in Earth Science, 3: 83.

Pritchard, M.E. & Simons, M. (2004). An InSAR-based survey of volcanic deformation in the central Andes. Geochemistry Geophysics Geosystems, 5: 1–4. https://doi.org/10.1029/2003GC000610

Putirka, K.D. (2008). Thermometers and barometers for volcanic systems. Reviews in Mineralogy and Geochemistry, 69: 61–120. https://doi.org/10.2138/rmg.2008.69.3

Pyle, D.M. (1989). The thickness, volume and grainsize of tephra fall deposits. Bull Volcanol, 51: 1–15. https://doi.org/10.1007/BF01086757

Ramón Folch, J.A. de (1954). Descubrimiento de Chile y compañeros de Almagro. Universidad Católica de Chile. Facultad de Filosofía y Letras. Instituto de Investigaciones Históricas, Santiago de Chile, 190 pp.

Ratto, N. (2013). A modo de introducción: la articulación de estudios arqueológicos, paleoambientales e históricos en el oeste tinogasteño (Catamarca). In: Delineando prácticas de la gente del pasado: Los procesos socio-históricos del oeste catamarqueño (Ratto, N., ed.). Sociedad Argentina de Antropología, Buenos Aires, 17–44.

Ridolfi, F. & Renzulli, A. (2012). Calcic amphiboles in calc-alkaline and alkaline magmas: thermobarometric and chemometric empirical equations valid up to 1,130°C and 2.2 GPa. Contributions to Mineralogy and Petrology, 163: 877–895.

Ridolfi, F.; Renzulli, A. & Puerini, M. (2010). Stability and chemical equilibrium of amphibole in calc-alkaline magmas: an overview, new thermobarometric formulations and application to subduction-related volcanoes. Contributions to Mineralogy and Petrology, 160: 45–66. https://doi.org/10.1007/s00410-009-0465-7

Roberge, J.; De Silva, S.; Viramonte, J.G.; Arnosio, M. & Beccio, R. (2012). Magma dynamics of the Cerro Blanco Volcanic Complex, Argentina, based on volatiles, major and trace elements in melt inclusions. Cordilleran Section, GSA 108th Annual Meeting, Paper No. 18-11.

Ruggieri, F.; Fernandez-Turiel, J.L.; Saavedra, J.; Gimeno, D.; Polanco, E.; Amigo, A.; Galindo, G. & Caselli, A. (2012). Contribution of volcanic ashes to the regional geochemical balance: The 2008 eruption of Chaitén volcano, Southern Chile. Science of the Total Environment, 425: 75–88. https://doi.org/10.1016/j.scitotenv.2012.03.011

Ruggieri, F.; Saavedra, J.; Fernandez-Turiel, J.L.; Gimeno, D. & Garcia-Valles, M. (2010). Environmental geochemistry of ancient volcanic ashes. Journal of Hazardous Materials, 183: 353–365. https://doi.org/10.1016/j.jhazmat.2010.07.032

Sampietro Vattuone, M.M.; Peña-Monné, J.L.; Maldonado, M.G.; Sancho Marcén, C.; Báez, W.; Sola, A. & Blasi, A. (2018). Cambios ambientales durante el Holoceno superior registrados en secuencias morfosedimentarias fluvio-eólicas del Valle de Santa María (Noroeste Argentino). Boletín Geológico y Minero, 129: 647–669. https://doi.org/10.21701/bolgeomin.129.4.004

Sampietro-Vattuone, M.M. & Peña-Monné, J.L. (2016). Geomorphological dynamic changes during the Holocene through ephemeral stream analyses from Northwest Argentina. Catena, 147: 663–677. https://doi.org/10.1016/j.catena.2016.08.029

Sarna-Wojcicki, A.M.; Shipley, S.; Waitt, R.B.; Dzurisin, D. & Wood, S.H. (1982). Areal distribution,

thickness, mass, volume, and grain size of air-fall ash from the six major eruptions of 1980. In: The 1980 eruptions of Mount St. Helens, Washington (Lipman, W. P. & Mullineaux, D. R., eds.). USGS, Washington, Prof. Paper, 1250: 577–600.

Scasso, R.A.; Corbella, H. & Tiberi, P. (1994). Sedimentological analysis of the tephra from the 12-15 august 1991 eruption of Hudson volcano. Bulletin of Volcanology, 56: 121–132.

Schindlbeck, J.C.; Freundt, A. & Kutterolf, S. (2014). Major changes in the post-glacial evolution of magmatic compositions and pre-eruptive conditions of Llaima Volcano, Andean Southern Volcanic Zone, Chile. Bulletin of Volcanology, 76: 830. https://doi.org/10.1007/s00445-014-0830-x

Seggiaro, R.; Hongn, F.; Folguera, A. & Clavero, J. (2000). Hoja Geológica 2769-II. Paso de San Francisco. Programa Nacional de Cartas Geológicas 1:250.000. 52 pp.

Sorem, R.K. (1982). Volcanic ash clusters: Tephra rafts and scavengers. Journal of Volcanology and Geothermal Research, 13: 63–71. https://doi.org/10.1016/0377-0273(82)90019-1

Stern, C.R. (2004). Active Andean volcanism: its geologic and tectonic setting. Revista Geologica De Chile, 31: 161–206. https://doi.org/10.4067/S0716-02082004000200001

Stern, C.R. (2008). Holocene tephrochronology record of large explosive eruptions in the southernmost Patagonian Andes. Bulletin of Volcanology, 70: 435–454. https://doi.org/10.1007/s00445-007-0148-z

Tilling, R.I. (2009). Volcanism and associated hazards: the Andean perspective. Adv. Geosci., 22: 125–137. https://doi.org/10.5194/adgeo-22-125-2009

Tomiya, A. & Takahashi, E. (2005). Evolution of the Magma Chamber beneath Usu Volcano since 1663: a Natural Laboratory for Observing Changing Phenocryst Compositions and Textures. Journal of Petrology, 46: 2395–2426. https://doi.org/10.1093/petrology/egi057

Trauth, M.H.; Bookhagen, B.; Marwan, N. & Strecker, M.R. (2003). Multiple landslide clusters record Quaternary climate changes in the northwestern Argentine Andes. Palaeogeography, Palaeoclimatology, Palaeoecology, 194: 109–121. https://doi.org/10.1016/S0031-0182(03)00273-6

Vidal, C.M. et al. (2015). Dynamics of the major plinian eruption of Samalas in 1257 A.D. (Lombok, Indonesia). Bulletin of Volcanology, 77: 73. https://doi.org/10.1007/s00445-015-0960-9

Viramonte, J.G.; Castro Godoy, S.; Arnosio, J.M.; Becchio, R. & Poodts, M. (2005). El campo geotermal de la caldera de Cerro Blanco: utilización de imágenes ASTER. XVI Congreso Geológico Argentino, 505–512.

Watanabe, K.; Ono, K.; Sakaguchi, K.; Takada, A. & Hoshizumi, H. (1999). Co-ignimbrite ash-fall deposits of the 1991 eruptions of Fugen-dake, Unzen Volcano, Japan. Journal of Volcanology and Geothermal Research, 89: 95–112. https://doi.org/10.1016/S0377-0273(98)00126-7

Watt, S.F.L.; Gilbert, J.S.; Folch, A.; Phillips, J.C. & Cai, X.M. (2015). An example of enhanced tephra deposition driven by topographically induced atmospheric turbulence. Bulletin of Volcanology, 77: 35. https://doi.org/10.1007/s00445-015-0927-x

Watt, S.F.L.; Pyle, D.M.; Mather, T.A.; Martin, R.S. & Matthews, N.E. (2009). Fallout and distribution of volcanic ash over Argentina following the May 2008 explosive eruption of Chaiten, Chile. Journal of Geophysical Research-Solid Earth, 114. https://doi.org/10.1029/2008JB006219

Wayne, W.J. (1999). The Alemania rockfall dam: A record of a mid-holocene earthquake and catastrophic flood in northwestern Argentina. Geomorphology, 27: 295–306. https://doi.org/10.1016/S0169-555X(98)00080-4

Wiesner, M.G.; Wetzel, A.; Catane, S.G.; Listanco, E.L. & Mirabueno, H.T. (2004). Grain size, areal thickness distribution and controls on sedimentation of the 1991 Mount Pinatubo tephra layer in the South China Sea. Bulletin of Volcanology, 66: 226–242. https://doi.org/10.1007/s00445-003-0306-x

Wilson, G.; Wilson, T.M.; Deligne, N.I. & Cole, J.W. (2014). Volcanic hazard impacts to critical infrastructure: A review. Journal of Volcanology and Geothermal Research, 286: 148–182. https://doi.org/10.1016/j.jvolgeores.2014.08.030

Yazdanparast, M.; Voosoghi, B. & Mossaiby, F. (2017). Determination of Cerro Blanco volcano deformation field using method of fundamental solutions. Geomatics, Natural Hazards and Risk, 8: 1258–1275. https://doi.org/10.1080/19475705.2017.1310765